2015

CO2 and O2 variability in the partially ice-covered Arctic Ocean

ASM F. Islam
University of Montana - Missoula

CO_2 AND O_2 VARIABILITY IN THE PARTIALLY ICE COVERED ARCTIC OCEAN

By
ASM FAKHRUL ISLAM

Bachelor of Science, University of Dhaka, Dhaka, Bangladesh, 2009

Masters Thesis
presented in partial fulfillment of the requirements
for the degree of

Master of Science
in Chemistry, Analytical and Environmental Chemistry

The University of Montana
Missoula, MT

July 2015

Approved by:

Dr. J.B. Alexander Ross, Dean of The Graduate School
Graduate School

Dr. Michael DeGrandpre, Committee chairperson
Department of Chemistry and Biochemistry

Dr. J.B. Alexander Ross, Committee member
Department of Chemistry and Biochemistry

Dr. Robert Yokelson, Committee member
Department of Chemistry and Biochemistry

Islam, ASM, M.S., July 2015 Chemistry

CO_2 and O_2 variability in the partially ice-covered Arctic Ocean

Chairperson: Dr. Michael DeGrandpre

Limited carbon cycle research has been conducted so far in the Arctic Ocean (AO) compared to many other open-ocean and coastal environments, with relatively few studies of the inorganic carbon cycle and air-sea gas exchange. Understanding these processes in depth and understanding the physical, chemical, and biological processes that control carbon dioxide (CO_2) and dissolved oxygen (DO) variability in the AO are crucial to predicting the future of the carbon cycle in the region and its impact on greenhouse gases and marine ecosystem processes, such as ocean acidification. To study the AO carbon cycle, *in situ* time-series data have been collected from the Canada Basin of the AO during late summer to autumn of 2012. Partial pressure of CO_2 (pCO_2), DO concentration, temperature, salinity, and chlorophyll-a fluorescence (Chl-*a*) were measured at 6-10 m depth under little ice and multi-year ice on two drifting platforms. The pCO_2 levels were always below atmospheric saturation, whereas the seawater was almost always slightly supersaturated with respect to DO. Although the two time-series data were on an average only 222 km apart they had 10 ± 10% and 63 ± 16% ice cover and differed significantly in contributions from gas exchange and net community production (NCP). Modeled variability of CO_2 and DO suggest that gas exchange, NCP and horizontal gradients are the main sources of the CO_2 and DO variability in the partially ice-covered AO. Horizontal gradients dominated the more densely ice-covered region, with no significant NCP in the surface. These results suggest that the signature imparted on CO_2 and DO in open water is widely disbursed under-ice and that biological production under multi-year ice is negligible due to lack of light and nutrients.

Acknowledgements

First and foremost, I would like to thank my advisor Dr. Michael DeGrandpre for his continual support and for accepting me into his lab in the first place. At the time I joined his lab I had zero knowledge of oceanography, but his ungrudging mentorship helped me get through the challenges and overcome the hurdles. Honestly, showing up in his office with all kinds of questions and getting answers with written explanations, when necessary, was something I did not expect. Besides his cordial mentorship, he has also been a caring guardian to me. His small actions like encouraging going out and having fun helped me feel at home and comfortable. In my three-year period in his lab I have learned how to work hard, at the same time, how to balance between professional and personal lives. In all honesty, I would like to express my utmost gratitude to him for all his care and support.

I thank Cory Beatty for agreeing to share his office with me and for being such a helping hand and good friend. He has been the most supportive man-next-desk I have ever had in my life. Had he not answered my stupid questions even as to how to use Microsoft Excel in my earlier days my journey of research could have been a nightmare. Also, it was him whom I picked to learn about American culture and lifestyle in further details. I will definitely cherish the teasing and chattering we used to have in room 318 for the rest of my life. I thank him for being such a good buddy.

I want to thank all of my co-workers in the DeGrandpre lab for their help and support. I thank the Department of Chemistry and Biochemistry for offering me admission and giving me the opportunity to be a proud member of the Grizzly family.

I would like to express my appreciation to my family members for their continual love and support. I would like to express my special gratitude to my parents without whom I would have never been able to make it all the way from the other side of the world, Bangladesh, to the United States.

Table of Contents

List of Figures

List of Tables

Chapter 1

Introduction

1.1. Overview

The Arctic Ocean (AO) is changing rapidly. Decrease in sea ice thickness (Perovich *et al.*, 2003, 2007; Maslanik *et al.*, 2007), freshening of the sea surface (Yamamoto-Kawai *et al.*, 2009a), changing mixed-layer dynamics (Toole *et al.*, 2010) and increased primary production (Arrigo and van Dijken, 2012) provide evidence that steady state conditions no longer exist in the AO. Recent decreases in Arctic summer sea ice area have also increased exchange of CO_2 and DO between the atmosphere and the ocean. Ocean acidification might be accelerated as ice cover decreases, potentially resulting in the largest and most rapid pH decrease of all the ocean basins during this century (Steinacher *et al.*, 2009). While most previous observations have found large pCO_2 undersaturation, there is evidence that loss of ice cover has already increased pCO_2 levels in AO surface waters (Cai *et al.*, 2010; Else *et al.*, 2013). It remains uncertain, however, whether the deep AO basins will uptake significant CO_2 under seasonal ice-free conditions. Rapid equilibration and warming of the shallow isolated surface water and weak biological CO_2 drawdown are hypothesized to limit CO_2 invasion, keeping the ice-free central AO basins from becoming large atmospheric CO_2 sinks (Cai *et al.*, 2010). The net effects of all these climate change impacts are unknown, but they show clear evidence of significant biogeochemical changes in the AO.

1.2. AO and Canada Basin

The Arctic Ocean is nearly landlocked, almost completely surrounded by Eurasia and North America (Fig. 1.0). It makes up ~4.3% of the ocean area but only ~1.4% of the volume (Jakobsson, 2002). The AO consists of a deep ocean basin, the broad shelves of the Barents, Kara, Laptev, East Siberian, Chukchi, Beaufort, White and Lincoln Seas and the narrow shelf off the Canadian Arctic Archipelago and northern Greenland (Fig. 1.0). The AO is partly covered by sea ice throughout the year and almost completely covered in winter. The surface temperature and salinity of the AO vary as the ice cover melts and freezes (Aagaard and Woodgate, 2001). Its salinity is the lowest compared to other oceans, due to low evaporation, heavy fresh water inflow, ice melt, and limited connection to nearby oceans that have comparatively higher salinities.

The Canada Basin is the largest sub-basin of the Arctic Ocean, extending approximately 1100 km from the Beaufort Sea shelf to the Canadian Archipelago (Fig. 1.0), with an average depth of 3800 m. Studying the Canada Basin of the AO has become particularly important due to its uniqueness in several respects (McLaughlin *et al.*, 2011). The Canada Basin is unique compared to other ocean basins in that it is surrounded by relatively broad and shallow (<200 m deep) continental shelves that comprise about 53% of the area of the AO (Bates and Mathis, 2009). The surface transpolar drift separates waters of the Canada Basin in the central basin of the AO from the Eurasian Basin. Its surface waters and subsurface halocline waters have distinctly different physical and chemical properties compared to the other basins. Warm and salty water from the North Atlantic enters the Canada Basin and forms the layer between about 250 and 800 m beneath the relatively cold Pacific water layer (Timmermans *et al.*, 2008). The loss of both multiyear and first-year ice is greater in the Canada Basin com-

pared to the other three sub-basins in the AO (McLaughlin *et al.*, 2011), making it more vulnerable to climate change.

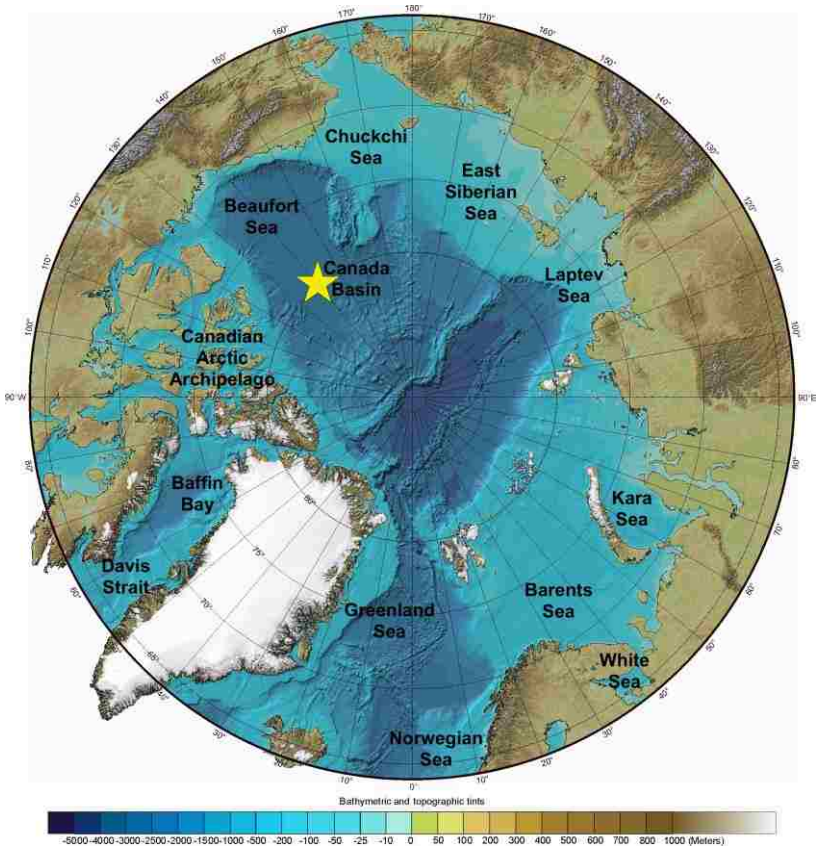

Figure 1.0 The International Bathymetric Chart of the Arctic Ocean (IBCAO, Jakobsson *et al.*, 2000) showing the Arctic marine regions. The study area is highlighted by the yellow star.

1.3. CO_2 and DO in the AO

The lack of long-term time-series data from the AO has limited scientists' understanding of the CO_2 sources and sinks and inorganic carbon cycling in the AO. Sea surface pCO_2 data sets from the central AO are scarce with most Arctic studies focused on nearshore and shelf areas (Anderson *et al.*, 2009; Bates *et al.*, 2006, Murata and Takizawa, 2003; Kaltin and Anderson, 2005). Anderson and Kaltin (2001) reported 250-300 μatm pCO_2 in the Eurasian Basin surface waters in August 1996. Over the time period of 1991 to 2005, Jutterström and Anderson (2010) found that all waters in the central AO are undersaturated with values typically below 300 μatm. Low pCO_2 values of 240-280 μatm have been observed in the Canada Basin adjacent to the Chukchi Sea shelf during summer 2002 (Bates, 2006; Bates et al., 2006), whereas 160-280 μatm pCO_2 have been observed along the sea-ice edge of the Chukchi and Beaufort Seas during September (Pipko et al., 2002; Murata and Takizawa, 2003). Fransson *et al.* (2009) reported lower surface seawater pCO_2 values of 150–250 μatm in the Makarov Basin of the Canada Basin from the summer of 2005. Cai *et al.* (2010) reported 250-365 μatm pCO_2 in the Canada Basin during summer 2008. Else *et al.* (2013) reported ~290-320 μatm pCO_2 beneath heavily decayed ice cover in the southeastern Canada Basin of the AO from early September of 2009. In the course of the late-summer 2011, Robbins *et al.* (2013) measured 322 μatm pCO_2 in the surface waters of the Canada Basin. All of these studies are summarized in Table 1.0.

Table 1.0. List of some previous studies of pCO_2 in or near the Canada Basin of the AO. Our measured pCO_2 values in open seawater and under multiyear ice coverage in the Canada Basin are typical of previous reports in the region. The list of the studies summarized below proceeds chronologically from top to bottom.

Study	**Time period**	**Region**	***p*CO$_2$ (μatm)**
Anderson and Kaltin (2001)	August 1996	Eurasian Basin	250-300
Jutterström and Anderson (2010)	From 1991 to 2005	Central Arctic Ocean	< 300
Bates (2006) Bates *et al.* (2006)	Summer 2002	Canada Basin (adjacent to the Chukchi Sea shelf)	240-280
Pipko *et al.* (2002) Murata and Takizawa (2003)	Summer 2002	Chukchi and Beaufort Seas (along the sea-ice edge)	160-280
Fransson *et al.* (2009)	Summer 2005	Makarov Basin	150–250
Cai *et al.* (2010)	Summer 2008	Canada Basin	250-365
Else *et al.* (2013)	Late summer 2009	Southeastern Canada Basin (beneath heavily decayed ice cover)	290-320
Robbins *et al.* (2013)	Late-summer 2011	Canada Basin	247-555
Our study	Late-summer to fall 2012	Canada Basin	**270-330**

Dissolved O_2 (DO) is an important climate parameter and is a key measurement for understanding the processes that control the marine carbon cycle and CO_2 variability. DO saturation in the ocean is predicted to decline by 4 to 7% by the end of this century because of climate change (Bopp *et al.*, 2002; Matear *et al.*, 2000; Plattner *et al.*, 2001; Sarmiento *et al.*, 1998). Recent reduction in DO in lower-latitude oceans (e.g., Johnson and Gruber 2007; Mecking *et al.*, 2008; Stramma *et al.*, 2008) may be linked to global climate change, which is also relevant to a warming and freshening AO (Proshutinsky *et al.*, 2009). According to available data, the central AO surface mixed layer is typically 2-3% of atmospheric saturation with DO maxima in the halocline (Falkner *et al.*, 2005). Low concentrations around 90% of saturation have been reported under winter sea ice cover in the southernmost Canada Basin (Sherr and Sherr, 2003). Sherr and Sherr (2003) observed a subsurface DO peak (>400 μmol kg^{-1}) during November 1997 in south-central Canada Basin. Hill and Cota (2005) observed supersaturation of DO in the Canada Basin during the spring and summer of 2002. Timmermans *et al.* (2010) observed a subsurface DO maximum consistently around 100% saturation between August and December 2008 in the Canada Basin.

Almost all of the pCO_2 and DO studies cited above were based on ships collecting data during the low ice periods in the summer. There continue to be significant gaps in our understanding of CO_2 and DO dynamics in the AO, especially under ice. To examine pCO_2 and DO variability in the AO, we deployed pCO_2, DO, temperature, salinity, Chl-*a*, and PAR sensors on ice-tethered profilers (ITPs) as part of the Joint Ocean Ice Study (JOIS) 2012 cruise. In 2012, the AO reached the lowest seasonal ice extent since the satellites began quantifying ice coverage in 1979 (Parkinson *et al.*, 2013; Zhang *et al.*, 2013). The most notable event in 2012 was a very strong storm that swept over the central AO in early August, rapidly enhanc-

ing ice melt and decreasing ice thickness (Parkinson *et al.*, 2013). Our sensors were deployed in late August, a few weeks after the storm and a couple of weeks before the ice extent reached its minimum on September 16. The two instrument packages were deployed in densely and sparsely ice-covered locations, providing a unique opportunity to compare CO_2 and DO variability under these different conditions. My research objective is to better understand the CO_2 and O_2 variability in the region through exploring the following questions:

(1) What is the open-water and under-ice *p*CO_2 and O_2 variability?

(2) What controls the variability of *p*CO_2 and O_2?

(3) Is the AO a net source or sink for atmospheric CO_2?

(4) What implications does the changing Arctic have for air-sea CO_2 fluxes, ocean acidification and biological production?

These questions will be examined in detail by use of correlative relationships, modeling and time-series (bandpass filtering) analysis.

Chapter 2

Methods

2.1. Study Site

Our instrumentation was deployed on two ITPs (ITP-64 and ITP-65) (Toole *et al.*, 2011; Krishfield *et al.*, 2008) (Fig. 2.1 and 2.2) in the Canada Basin as part of the Beaufort Gyre Observing System (BGOS) study during the JOIS 2012 cruise on the Canadian Coast Guard Icebreaker (CCGS) Louis S. St. Laurent. ITP-65 was deployed on a 1.5 m thick ice floe on August 27, 2012 at 80° 53.4 N, 137° 25.8 W and ITP-64 was deployed in open water because of limited ice extent on August 28, 2012 at 78° 46.5 N, 136° 39.8 W (Fig. 2.1). The two drifters were initially 245 km away from each other (Fig. 2.1). The ITPs followed the ice flow, as a result, ITP-64 and ITP-65 traveled 513 and 575 km, respectively, during the period when the sensors transmitted data (Fig. 2.1).

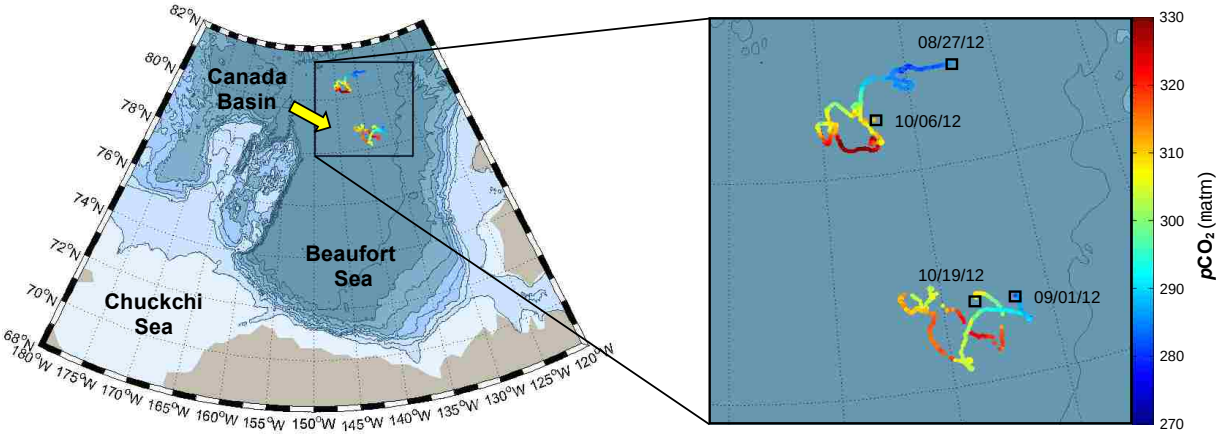

Figure 2.1. Arctic marine regions (left) near the study area (inset) are shown with the ITP drift track overlaid. The study area is magnified on the right figure. Measurement start and end points are highlighted by rectangular boxes labeled with dates. pCO_2 values at different points over the drift track are shown in color. The top track corresponds to ITP-65 and the bottom track to ITP-64. The sensors were deployed roughly 245 km away from each other. Plotting software is courtesy of Bill Williams (Institute of Ocean Sciences, Canada).

2.2. *In situ* Sensors

2.2.1. The ITP

The ITPs (Krishfield *et al.*, 2008a) consist of 1) a surface buoy that houses an inductive modem, GPS receiver and Iridium satellite phone; 2) a weighted, jacketed, wire rope that extends to the end of the profiling range; and 3) an instrumented profiler (McLane Research Laboratories Inc.) containing a CTD (SBE41CP, Sea-Bird Electronics Inc.), DO sensor (SBE43I, Sea-Bird Electronics Inc.) and bio-optical package (Fig. 2.2).

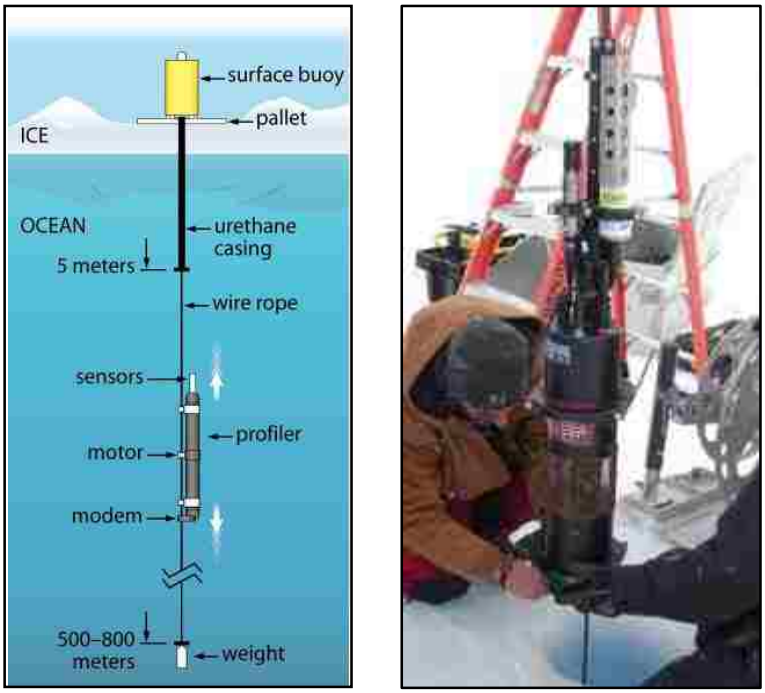

Figure 2.2. ITP schematic (left) and SAMI tethered ITP deployment through the ice (right). The SAMI sensor (black cylinder) is located at 6 m depth directly below the urethane casing ~2-4 m below the ice (not shown). The CTD and DO sensors are located above the SAMI (right and left silver housings, respectively). ITP schematic was obtained from WHOI website: http://www.whoi.edu /page.do?pid=23099.

All data collected by the ITPs were transmitted to the surface with inductive modems and telemetered via Iridium satellite. The transmitted data were downloaded, processed, and made available at the Woods Hole Oceanographic Institution (WHOI) website. The ITPs profiled between ~11-800 m depth with 4 profiles per day.

2.2.2. SAMI-CO_2

Two Submersible Autonomous Moored Instruments for CO_2 (SAMI-CO_2, Sunburst Sensors, LLC) (Fig. 2.3) were used to measure pCO_2 in seawater (SAMI-12 and SAMI-14). The SAMI uses pH indicators to quantify pCO_2. The quantification is done through equilibration with a pH indicator solution contained within a gas permeable membrane (DeGrandpre *et al.*, 1995, 1999). The equilibrated solution is pumped into an optical cell where the absorbance of the indicator is measured at specific wavelengths (Fig. 2.3). With the pH indicator solution renewed for each measurement and the optical blanks measured intermittently, the SAMI-CO_2 has no detectable drift (DeGrandpre *et al.*, 1995, 1999). The sensors were calibrated in our lab and tested with the ITP off the WHOI dock prior to deployment. SAMI-CO_2 are free from field calibration and are capable of operating at low temperatures of Arctic waters by adding ethylene glycol to the indicator and the blank solutions. Before deployment, each SAMI was calibrated using standard calibration gases over the pCO_2 range of interest at the expected average *in situ* temperature (DeGrandpre *et al.*, 1995). Both SAMIs we deployed were connected to the ITP wire at ~6 m depth and recorded the pCO_2 at 2 hour intervals. SAMIs passed all data to the surface controller through an inductive modem interface (SBE UIMM 350 m). For unknown reasons, the SAMI inductive modem communications failed on both ITPs and the time-series for ITP-64 and ITP65 were limited to 49 and 41 days, respectively.

Figure 2.3. The SAMI-CO_2 sensor is shown on left. The right picture shows the sensor part of the SAMI (optical cell and membrane equilibrator). Pictures obtained from Sunburst Sensors website.

2.2.3. Ancillary Sensors

The SAMIs were interfaced with O_2 sensors (Optode 4175, Aanderaa Data Instruments) and a conductivity, temperature, and depth (CTD) sensor (SBE37SI, Sea Bird Electronics Inc.) (Fig. 2.4). The CO_2, O_2, and CTD sensors were distributed on the wire rope with depths differing by <0.5 m (Fig. 2.2). SAMIs passed all ancillary sensor data to the surface controller through an inductive modem interface (SBE UIMM 350 m). The O_2 sensors were calibrated in the lab using both an air-saturated solution and a zero oxygen solution at room temperature. All instruments were tested off the WHOI dock prior to deployment. Like the SAMIs, the profilers were configured with CTD sensors (SBE41CP, Sea-Bird Electronics Inc.) that had an integrated dissolved O_2 sensor (SBE43I, Sea-Bird Electronics Inc.) and a full bio-optical system mounted at the very top of the endcap of the profiler. The bio-optical package included an irradiance detector (PAR-LOG, Satlantic Inc.) that recorded the intensity of the photosynthetically active radiation (PAR) and a customized 'triplet' fluorometer (ECO FLbb-CD, WETLabs Inc.) that measured chlorophyll fluorescence (Chl-*a*), colored dissolved organic matter fluorescence and optical backscatter (Laney *et al.*, 2014). All bio-optical sensors were calibrated separately as described by Laney *et al.* (2014). Calibration details of oth-

er sensors on the profilers are summarized in Krishfield *et al.* (2008b). PAR sensor was not calibrated or had other problems.

Figure 2.4. Sensors deployed with the SAMI or on the profiler: Aanderaa oxygen sensor (on SAMI) (top left), Microcat CTD sensor (on SAMI) (top right), Satlantic PAR sensor (on profiler) (bottom left), and WETLabs Chl-*a* sensor (on profiler) (bottom right).

2.3. Ancillary Data

A variety of other data were collected from different platforms or Internet sources. The wind speed data near ITP locations were obtained from the European Center for Medium range Weather Forecasting *(*ECMWF*)* website: http://apps.ecmwf.int/datasets/data/interim-full-daily. Barometric pressure and air temperature data were obtained from the Ice-Mass Balance (IMB) Buoy website: http://imb.erdc.dren.mil/2012L.htm. Hourly average mole fractions of atmospheric CO_2 (xCO_2) measured at Barrow, Alaska were obtained from the National Oceanic and Atmospheric Administration (NOAA) Earth System Research Laboratory (ESRL) website: http://www.esrl.noaa.gov/gmd/dv/ data/. Ice coverage data were obtained from the National Snow and Ice Data Center (NSIDC): http://nsidc.org/data. The PAR data from the sensors mounted on the ITPs was uncalibrated, so we used surface solar radiation

that corresponded to the ITP locations computed at 7.5 minute intervals. The PAR data were adjusted for light loss and scattering assuming an attenuation of 40% at ~9 m (Penta *et al.*, 2008).

2.4. Data validation

An underway pCO_2 equilibrator-infrared measurement system (SUPER-CO_2, Sunburst Sensors) (Fig. 2.5) provided validation data during the ITP deployment. In order for SUPER-CO_2 to be used as a reference for the SAMI, it required correction for warming inside the water line and equilibrator. The SUPER-CO_2 values were therefore corrected to the sea surface temperature using the following formula (Dickson *et al.*, 2007):

$$(pCO_2)_{Ts,wet} = (pCO_2)_{Te,wet} \times \exp[0.0423(T_s - T_e)] \qquad (2.1)$$

where T_s is the sea surface temperature, T_e is the temperature measured in the SUPER-CO_2 equilibrator.

After correction factors were applied on all SUPER pCO_2 values they were further compared to SAMI pCO_2 values collected during the time the ship was at the ITP location. SAMIs offsets were corrected accordingly. Once the initial shipboard data verifies SAMI accuracy at the time of deployment, there are very few mechanisms that can lead to drift and inaccuracy later on. Few primary known mechanisms include certain types of electronic problems, poor pump flushing, and biofouling. Issues related to electronics and pump flushing can be readily diagnosed via metadata transmitted with each SAMI measurement. Biofouling is not a significant problem with SAMI over the deployment period.

Figure 2.5. The SUPER-CO_2 system (Sunburst Sensors, LLC) was used to quality control the SAMI data. It is designed for automated shipboard analysis of seawater and atmospheric pCO_2. SUPER-CO_2 can take measurements at subsecond temporal resolution. Image obtained from Sunburst Sensors website.

Dissolved O_2 from both systems (SAMI and profiler) were quality controlled using the following procedure. The surface SAMI and profiler DO values at the beginning of the ITP deployment were corrected for offsets by comparing with surface shipboard DO measurements performed during the deployment (Winkler titration method). After the ship left the ITP location, the surface SAMI DO data were corrected for sensor drift by referencing to the profiler data corrected to the deep-water isopycnal (constant density) values (Timmermans *et al.*, 2010). The QC procedure is based on the assumption that DO variability on deep isopycnals is negligible (Timmermans *et al.*, 2010). For this purpose, the deep DO profiler values were first corrected with deep bottle data from the time of deployment and all subsequent deep values were corrected to these values by applying an offset, then the surface SAMI DO values were compared with the surface profiler values and corrected for offset.

SAMI temperatures were compared with SAMI-CTD temperatures and corrected for offset. Salinity measured by SAMI-CTD and profiler surface CTD agreed well so did not require correction.

2.4.1. Partial Pressure of carbon dioxide (pCO_2)

Temperature-corrected SUPER pCO_2 values and SAMI pCO_2 values at the beginning of the measurement were compared and a difference of 75 µatm and 21 µatm were observed for SAMI-12 and SAMI-14, respectively. In both cases, SAMIs were overestimating pCO_2 data and the data were corrected. The SAMI-12 had a leaky reagent bag, which was replaced prior to deployment and likely led to the large offset. After offsets were applied on all SAMI pCO_2 values, the data were further compared to SUPER pCO_2 values during the time the ship was at the SAMI locations. The mean difference ± standard deviation between the corrected SAMI pCO_2 and SUPER pCO_2 values were 1.3 ± 0.1 µatm (n=3) for ITP-64 and 0.3 ± 0.3 µatm (n=5) for ITP-65 (Fig. 2.6).

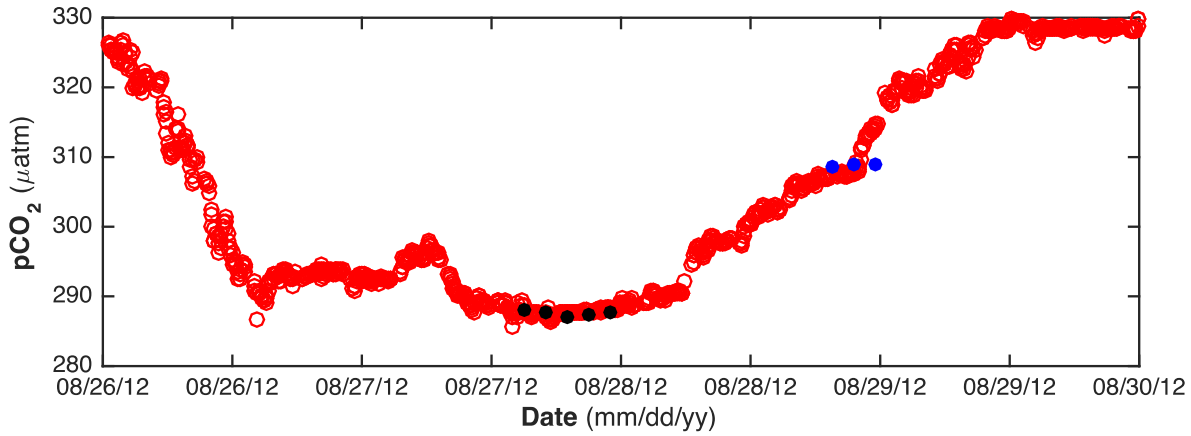

Figure 2.6. Discrete pCO_2 measured underway by SUPER system was used to quality control the SAMI CO_2 data. The blue (ITP-64) and black (ITP-65) filled symbols are SAMI pCO_2 data and the open red symbols are SUPER pCO_2 data. Corrected SAMI data overlaps SUPER data while the ship was at the ITP deployment location. The ship was moving to other locations between ITP deployments.

2.4.2. Dissolved Oxygen Concentration (DO)

As stated above, the optodes on SAMI-12 and SAMI-14 measured DO at 6 m depth at 2 hour intervals. Profiler-O_2 sensors (O_2 sensors on ITP-64 and ITP-65) took measurement along the water column down to ~800 m depth, but at ~11 m depth the measurements had 6-hour intervals. SAMI DO values at the beginning of the deployment were lower than the Winkler (ship) values by 31 μmol/kg and 23 μmol/kg for SAMI-12 and SAMI-14, respectively. Therefore, offset correction was applied to both data sets. The offset corrected SAMI DO data were then compared with offset and drift corrected ITP surface DO data (see next paragraph) to check for possible drift. A constant linear drift was observed with both SAMI-12 and SAMI-14 DO data (Fig. 2.7).

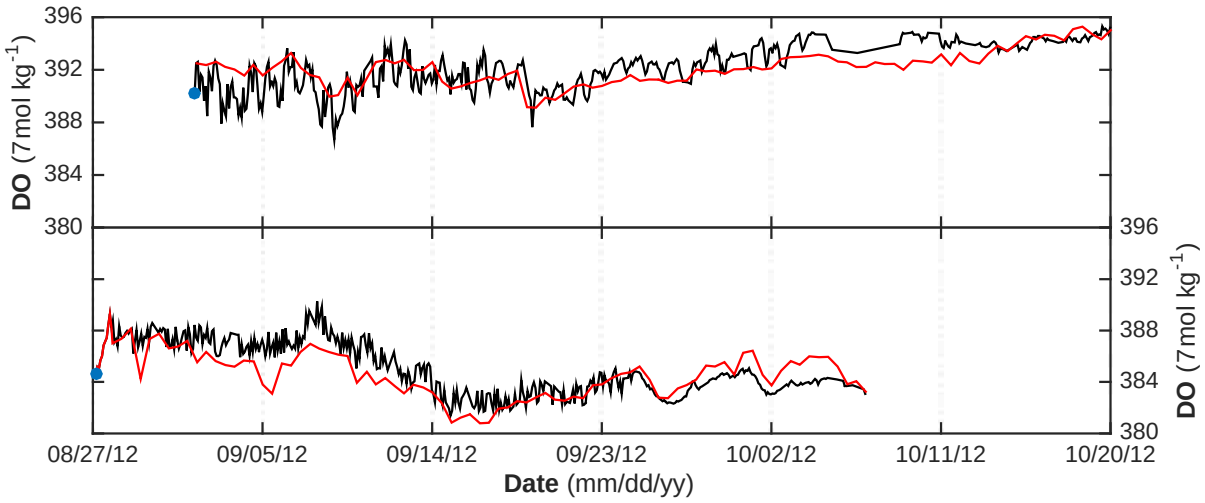

Figure 2.7. Profiler surface DO (red) and SAMI DO (black) at the beginning of the measurement were compared to surface shipboard DO measurements (blue) performed at the time of the deployment. The top figure refers to ITP-64 and bottom figure refers to ITP-65. After correcting to the bottle data, SAMI DO was corrected to the profiler data. The SAMI DO data appear noisier than the profiler data because they measured every 2 hours, capturing the short-term variability. The profiler was at the surface only ~4 times per day.

Comparison of the profiler DO data with the shipboard data found an offset of 16 μmol/kg for ITP-64 and 2 μmol/kg for ITP-65. In both cases, the profiler DO values were lower than the ship DO values and were corrected accordingly. The offset-corrected profiler surface DO values were then compared with deep DO values, as described above. Based on this analysis, the optode sensors on the ITPs drifted by ~10 μmol/kg or less relative to the profiler data and offsets were applied accordingly (Fig. 2.7).

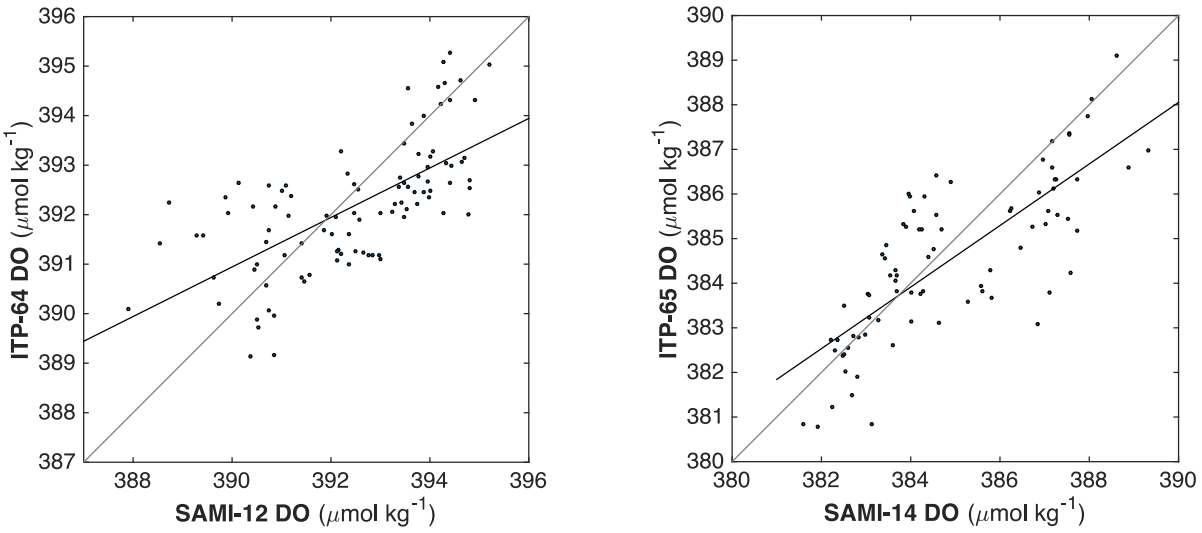

Figure 2.8. ITP-64 (left) and ITP-65 (right) profiler surface DO and SAMI DO correlation plots. Black lines refer to data correlation lines and gray lines refer to 1:1 lines. After offset and drift correction profiler surface DO and SAMI DO had r^2 values of 0.44 and 0.60, respectively, and a slope of 0.45 and 0.70, respectively. SAMIs measured DO at 6 m depth at 2 hour intervals and profilers measured DO at ~11 m depth at 6 hour intervals.

After applying offset and drift correction on SAMI and ITP DO data, the data sets better agree with each other (Fig. 2.8). There is considerable scatter primarily because this is very narrow range of DO variability, so any noise in the measurements would translate into scattering of data. Also, at times the SAMI and the profiler O_2 sensors might have encountered slightly different masses of water due to local processes at different depths (the two

instruments had <0.5 m depth difference). A correlation plot between SAMI-12 DO and profiler DO values gives r^2 = 0.44 and a slope of 0.45, and, that between SAMI-14 DO and profiler DO values gives r^2 = 0.60 and a slope of 0.70. After the correction the SAMI and shallowest ITP profile DO data compared to within ± 0.8 and ±0.7 μmol kg^{-1} for ITP-64 and ITP-65, respectively.

2.4.3. Temperature

SAMI-CO_2, surface CTD, and profiler CTD, all measured temperature. The first two took measurements at 2 hour intervals and the latter at 6 hour intervals at its shallowest depths (~11 m). Both SAMIs gave a constant temperature offset. Their temperatures were always 0.16 ^oC lower than the temperature measured by the CTDs mounted on them. The SAMI temperatures were corrected accordingly for offset because the CTD temperature was considered more accurate. After offset correction, the temperature data from both sensors agreed well (Fig. 2.9) with the mean difference and the standard deviation being small. A correlation plot between SAMI-12-CO_2 temperature and SAMI-12-CTD temperature gives r^2 = 0.87 and a slope of 0.90, and that between SAMI-14-CO_2 temperature and SAMI-14-CTD temperature gives r^2 = 0.85 and a slope of 0.84 (Fig. 2.9). After the correction, the SAMI and CTD data compared to within ± 0.009 and ±0.008 ^oC for ITP-64 and ITP-65, respectively. The SAMI-CO_2 temperatures were compared only with the SAMI-CTD temperatures because the CTD temperature was considered more accurate and the profiler CTDs were at different depths than the SAMIs. The profiler CTDs also had less measurement frequency at their shallowest depths compared to the SAMIs.

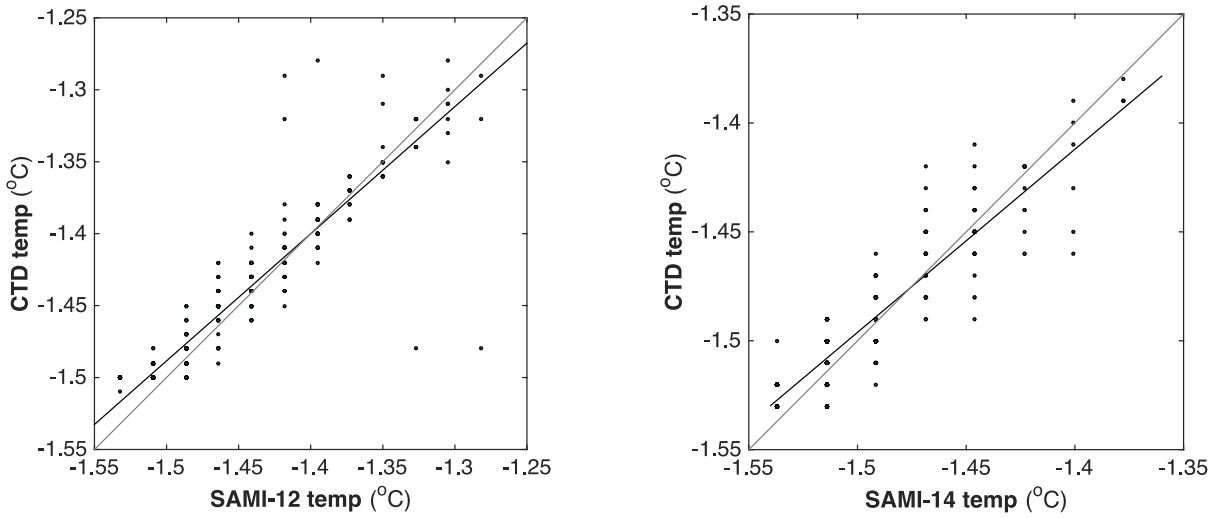

Figure 2.9. ITP-64 (left) and ITP-65 (right) CTD and SAMI temperature correlation plots. After correcting SAMI temperature for offsets the r^2 values were 0.87 and 0.85, respectively, and slopes were 0.90 and 0.84 respectively. Both SAMI and CTD on the SAMI took measurements at 2 hour intervals.

2.4.4. Salinity

SAMI-CTD and profiler-CTD measured salinity at 6 m and ~11 m depth at 2 hour and 6 hour intervals, respectively. The data from the sensors agreed well so did not require any correction (Fig. 2.10). SAMI-CTD and profiler-CTD data compared to within ± 0.006 and ±0.008 units for ITP-64 and ITP-65, respectively. A correlation plot between ITP-64 salinity and SAMI-12 salinity gives $r^2 = 0.62$ and a slope of 0.62 and that between ITP-65 salinity and SAMI-14 salinity gives $r^2 = 0.98$ and a slope of 1.0. The correlation is 0.92 with a slope of 0.95 for ITP-64 and 0.99 with a slope of 1.0 for ITP-65 (Fig. 2.10) until the water approached the freezing temperature.

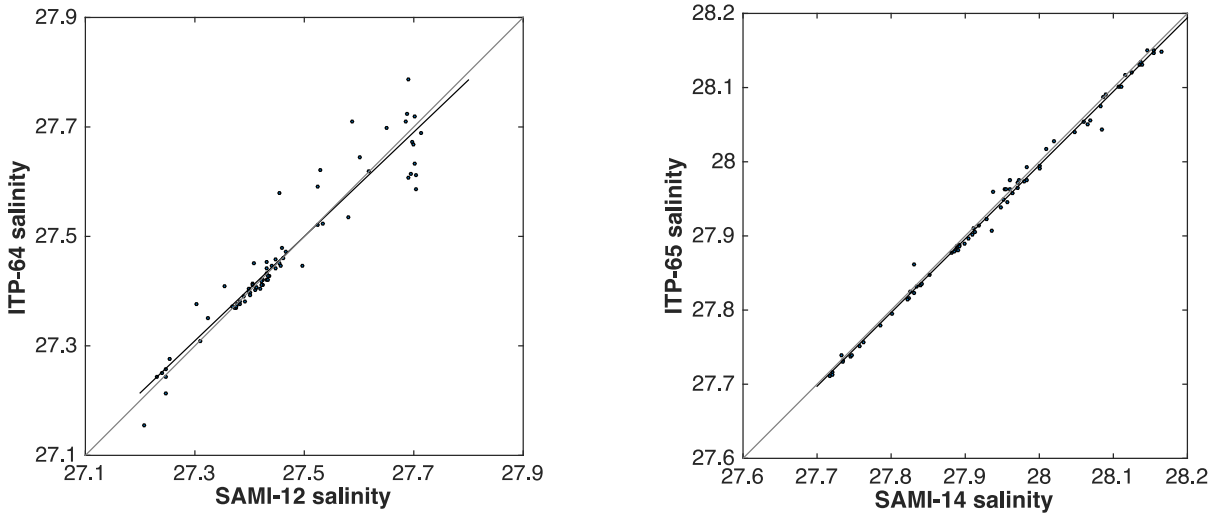

Figure 2.10. ITP-64 (left) and ITP-65 (right) profiler surface salinity and SAMI salinity correlation plots. The salinity data did not need offset and drift correction. The r^2 values until the water reached the freezing temperature are 0.92 and 0.99 for ITP-64 and ITP-65, respectively, and the slopes are 0.95 and 1.0, respectively. SAMI-CTD and profiler-CTD measured salinity at 6 m and ~11 m depth at 2 hour and 6 hour intervals, respectively.

2.4.5. Bio-optical parameters

Chl-*a* data were obtained by direct conversion of digital counts to concentration according to the manufacturer calibration sheets. Chl-*a* data from both profilers contained a number of outliers so appropriate ranges of tolerance were applied to both data sets to filter out the outliers. The surface solar radiation corresponding to the ITP locations was scaled using the surface PAR data collected on the ship to account for the nearly constant cloud cover and absorption due to seawater to 9 m.

2.5. Calculations

2.5.1. Water Density

Water density was calculated using *in situ* temperature and salinity data at corresponding depths. First, the density is calculated at one standard atmospheric pressure. Then the secant bulk modulus is calculated to get density under a given condition. The calculation is an

implementation of the International Equation of State of Sea Water, 1980 (IES80) taken from "Introductory Dynamical Oceanography" by Pond and Pickard (Appendix 3, pp 310-311).

2.5.2. Freezing Temperature of Water

In order to observe when ice formation could occur, the freezing point of seawater was calculated using *in situ* salinity data (Millero and Leung, 1976) according to the formula in Millero and Leung (1976).

2.5.3. Mixed Layer Depth (MLD)

The mixed layer depth (MLD) was calculated from depth-resolved density and temperature, with MLD as the depth where the density difference from the SAMI depth is +0.3 kg m^{-3} (Fig. 3.2). This value is close to the value of 0.26 kg m^{-3} found by Timmermans *et al.* (2010) using the same approach for the central Canada Basin. We used a density difference of 0.3 kg m^{-3} because it gives computed MLDs that best match *in situ* MLDs when observed visually based on the water column density profile.

2.5.4. Total Alkalinity (A_T)

Alkalinity was derived from a salinity-total alkalinity (A_T) relationship for the Chukchi Sea, Beaufort Sea, and Canada Basin (Yamamoto-Kawai *et al.*, 2005; Fig 2.11). The relationship was corrected for the influence of sea ice melting/formation and has a coefficient of 0.99. The corrected relationship was used; however, there are various mechanisms such as variable contributions of river runoff, sea ice meltwater (Ulfsbo *et al.*, 2014), carbonate mineral precipitation or dissolution (Cross *et al.*, 2013) that can introduce significant uncertainties to this conservative relationship.

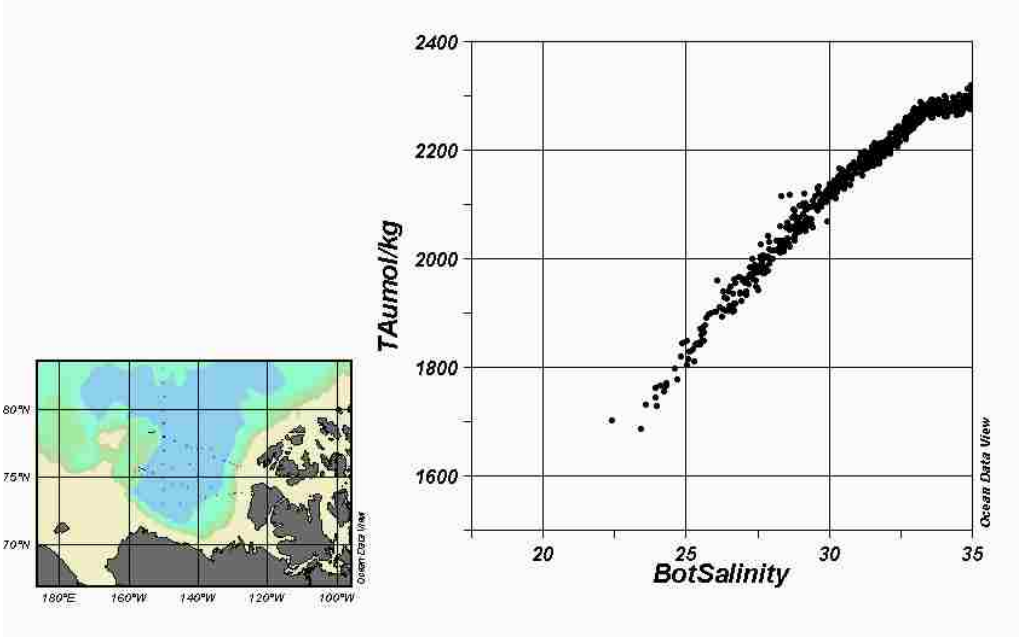

Figure 2.11. Historical Salinity-A_T (shown as TA in this figure) relationship (right) for the Canada Basin and Beaufort Sea (Yamamoto-Kawai *et al.*, 2005). The left figure refers to the location the salinity and alkalinity data were collected from.

Ulfsbo *et al.* (2014) found a mean difference between the measured and computed A_T of 4 ± 23 μmol kg^{-1}. The relationship overestimated A_T by ~30 μmol kg^{-1} in the Canada Basin and near the Laptev Sea, where the discrepancies were the largest. Our A_T was computed from ITP-64 and ITP-65 salinity using the following equation based on the historical Salinity-A_T relationship for the Canada Basin and Beaufort Sea by Yamamoto-Kawai *et al.* (2005):

$$A_T = 62.47 \times \text{Salinity} + 261.34 \qquad (2.2)$$

where A_T is in μmol kg^{-1} and S is *in situ* salinity (unitless).

2.5.5. Normalized DIC (nDIC)

Normalized DIC reduces the variability in DIC caused by riverine input of alkalinity and advective process. The normalization of DIC to a constant salinity (35) (Fig. 4.5) was done according to following formula:

$$nDIC = DIC \times (35/Salinity) \qquad (2.3)$$

where DIC is *in situ* DIC (in μmol kg^{-1}) and Salinity is *in situ* Salinity.

2.5.6. Equilibrium O_2 Concentration in Seawater

Saturated DO is the dissolved amount of O_2 in seawater in equilibrium with the atmosphere, but it is the partial pressure that controls the gas exchange. Consequently, the water vapor reduces the partial pressure of O_2 and needs to be accounted for in gas exchange calculations. DO saturation values were calculated using *in situ* temperature, salinity and barometric pressure with water vapor pressure accounted for using equations in Gnaiger and Forstner (1983). Salty water vapor pressure was calculated at *in situ* temperature and salinity and O_2 solubility was calculated from temperature, salinity and barometric pressure (Gnaiger and Forstner, 1983). Equilibrium O_2 concentration was then calculated using the following formula:

$$O_2 \text{ (equilibrium } O_2 \text{ concentration at } in\ situ \text{ T, S and P)} = O_2 \text{ } (O_2 \text{ saturation at } in\ situ \text{ T and S)} \times P[(1-P_w/P)\ (1-ThetaP)] / [(1-P_w)(1-Theta)] \qquad (2.4)$$

where, T is temperature (in ^oC), S is salinity (unitless), P is barometric pressure (in atm), P_w is the water vapor pressure (in atm), and

$$Theta = 0.000975 - (1.426 \text{ x } 10\text{-}5 \times T) + (6.436 \text{ x } 10\text{-}8 \times T^2) \qquad (2.5)$$

2.5.7. Atmospheric pCO_2 at the Sea Surface

xCO_2 data downloaded from the NOAA-ESRL website were multiplied by local barometric pressure to get pCO_2 in dry air. Atmospheric pCO_2 in wet air was then calculated by

including water vapor pressure (Dickson *et al.*, 2007) according to the following formula (Dickson *et al.*, 2007):

$$p(CO_2 \text{ at sea surface}) = p(CO_2 \text{ in dry air}) \times (1 - P_w) \qquad (2.6)$$

where, P_w is the water vapor pressure over the seawater sample of *in situ* salinity at the temperature of equilibration (Gnaiger and Forstner, 1983).

2.6. Modeling

2.6.1. Partial Pressure of carbon dioxide (pCO_2)

When carbon dioxide enters seawater it reacts with the water. The reactions can be represented by the following series of equilibria:

$$CO_2\,(g) \rightarrow H_2CO_3^*\,(aq) \qquad (2.7)$$

$$H_2CO_3^*\,(aq) \leftrightarrow H^+\,(aq) + HCO_3^-\,(aq) \qquad (2.8)$$

$$HCO_3^-\,(aq) \leftrightarrow H^+\,(aq) + CO_3^{2-}\,(aq) \qquad (2.9)$$

It is difficult to analytically distinguish between CO_2 (aq) and H_2CO_3 (aq) so both are combined and the sum is expressed as the concentration of a hypothetical species, $H_2CO_3^*$ (aq).

2.6.2. Dissolved Inorganic Carbon (DIC)

Total dissolved inorganic carbon (DIC), defined as the sum of concentrations of the different carbon species i.e. HCO_3^-, CO_3^{2-}, $H_2CO_3^*$ in seawater, was calculated using CO2SYS (Fig. 4.5) developed for CO_2 system calculations (van Heuven *et al.*, 2011): http://cdiac.ornl.gov/ftp/co2sys/. In our calculations, CO2SYS takes temperature, salinity, depth, pCO_2 and salinity-derived alkalinity (A_{Tsalin}) (protolytic nutrients e.g. phosphate are assumed to be negligible) as input and returns DIC and other CO_2 parameters as output, in-

cluding aragonite saturation (Ω_{arag}). The saturation state of seawater with respect to aragonite (a form of calcium carbonate found in plankton and invertebrates) can be defined as the product of the concentrations of dissolved calcium ions (Ca^{2+}) and carbonate ions (CO_3^{2-}) in seawater, at the *in situ* temperature, salinity, and pressure, divided by the stoichiometric solubility product (K^*_{sp}) for those conditions, according to the following equation:

$$\Omega_{arag} = ([Ca^{2+}] \times [CO_3^{2-}]) / K^*_{sp} \qquad (2.10)$$

2.6.3. Dissolved Oxygen Concentration (DO)

CO_2 and O_2 are intimately related through photosynthesis and respiration. Photosynthesis is the production of organic matter from inorganic carbon and respiration is the destruction of organic matter by reaction with oxygen in the presence of sunlight. The photosynthetic reaction, which represents the average stoichiometry of organic matter production based upon analysis of seawater, is:

$$106\ CO_2 + 16\ NO_3^- + HPO_4^{2-} + 122\ H_2O + 18\ H^+ \rightarrow \text{Organic matter} + 138\ O_2 \qquad (2.11)$$

In the process of photosynthesis, O_2 is produced while CO_2 is consumed, thus making the O_2 profile potentially a mirror image of the CO_2 profile in seawater. Therefore, DO is a very valuable counterpart to CO_2 as the two can be modeled using similar processes and divergence from model predictions or expected correlations provides additional insight into the controlling processes of the carbon cycle.

2.6.4. Temperature, Salinity

Sea surface temperature can be used as an indicator of various phenomena going on in the seawater based on the assumption that the anomalies of sea-surface temperature i.e. devia-

tion from the mean, indicates potential mixing of different water masses and sea surface heating and cooling due to air-sea exchange of heat and absorption of solar radiation. In the AO surface water, however, temperature hardly varies and is not a strong indicator of these processes.

In the AO, salinity differences in seawater tend to cause stronger stratification inhibiting vertical mixing of seawater in the water column. Evaporation (not prominent in the AO) and ice formation can cause an increase in salinity. When the seawater freezes it excludes salts from the ice through a process called "brine rejection" and the surrounding seawater becomes saltier and denser, sinking into the water column causing mixing. Saline water also holds less gas because some of the water molecules are occupied to dissolve the salt and these more concentrated dissolved gases sink down with the brine. Precipitation (rain) and ice melt are other sources of salinity variability causing a decrease in salinity by increasing the proportion of H_2O and diluting the concentrations of salts. Because these effects reduce density, they are more persistent at the air-sea interface and require a mixing mechanism such as wind or ice shear to dissipate.

2.6.5. Model Calculations

2.6.5.1. DIC and DO flux

The flux (changes over time) of DIC and DO potentially originate from 4 different processes in the AO as described in the following mass balance:

$$H \times \Delta C/\Delta t = F_{gasex} + F_{NCP} + F_{mix} + F_{brine} \qquad (2.12)$$

where H is the mixed layer depth, ΔC is the difference in DIC or DO values between two measurements over time Δt, and F_{gasex}, F_{NCP}, F_{mix}, and F_{brine} are the fluxes due to gas transfer

across the air-water interface, net community production (NCP), vertical mixing and advection, and brine rejection during ice-formation, respectively. We assume $CaCO_3$ dissolution and formation is not significant. If each of these processes can be modeled using established relationships and physical data, it is possible to quantitatively predict the overall variability in DIC and DO (e.g. DeGrandpre *et al.*, 2004). In this evaluation, we focus on calculation of F_{gasex} and F_{NCP} and the contribution of the other fluxes, which are more difficult to model, are estimated by examining the residual variability. The F_{gasex} of CO_2 and DO across the air-water interface was calculated using the diffusive boundary layer model:

$$F_{gasex} = k \, \Delta C \, (1\text{-}f) \qquad (2.13)$$

where k is the gas transfer velocity and f is the fractional ice coverage. k, which accounts for the rate of gas diffusion through the air-sea boundary layer, was estimated using a wind speed relationship and adjusted for different temperatures and gases (i.e., CO_2, DO) using the updated equation in Wanninkhof (2014):

$$k = 0.251 \, \langle U^2 \rangle \, (Sc/660)^{-1/2} \qquad (2.14)$$

where $\langle U^2 \rangle$ is average squared wind speed adjusted to 10 m height and Sc is the Schmidt number which accounts for differences in molecular diffusivity between gases. A negative F_{gasex} represents a flux from the atmosphere to the ocean.

Since air-sea gas flux in the Canada Basin is expected to be virtually insignificant for the most of the year due to significant ice cover, annual uptake of CO_2 (in Tg C yr^{-1}) was calculated as the product of late summer-autumn CO_2 flux (in mmol m^{-2} d^{-1}) and the corresponding area (in km^2). We assumed that gas flux is significant over a 90 day season when open water was significant.

We interpret short-term salinity changes that return to an earlier baseline to be primarily due to different water masses that advected past the non-Lagrangian (i.e. it did not follow the water) drifter (Timmermans *et al.*, 2012). Vertical mixing is assumed negligible due to the strong halocline (salinity stratification), as discussed below. The DIC and O_2 flux from brine formation were not modeled but their importance in these data can be assessed by comparison of the DO and DIC time-series, as discussed below.

We evaluated contributions of NCP in three ways: 1) by fitting the residual signal not accounted for by gas exchange; 2) revealing the diurnal signal by computing bandpass filtered DIC and DO, after removing the contribution of F_{gasex} and 3) by using a photosynthetic model (explained below). To obtain the bandpass filtered data, 4 hour low pass and 30 hour high pass filters were used to pull out the diurnal signal. The output is the hourly rate of change in DIC and DO. NCP from DO was compared with NCP from DIC by conversion with the photosynthetic quotient 1.4 (see Equation 2.11). Gross primary production (GPP) was then calculated by adding nighttime respiration to daytime NCP. Because influence of non-local advection appear in the NCP data (Fig. 4.4) as different water masses often contain different levels of CO_2 and DO, DIC and DO in seawater can change disparately when there are potential influence from non-local processes (DeGrandpre *et al.*, 1998). This is discussed in more detail below. Data corresponding to those time periods were omitted in the daily mean of NCP and GPP (Fig. 4.4), as discussed below.

2.6.5.2. Gas Exchange and NCP model

The mass balance (Equation 2.12) used two biogeochemical models for pCO_2 and DO. The pCO_2 model was generated using an in-house program for carbonate system calculations

(DeGrandpre *et al.*, 2004). The model takes the initial DIC and A_{Tsalin} at *in situ* temperature and salinity in the surface seawater as the initial input. DIC and A_{Tsalin} initial were 1878 and 1975 μmol kg^{-1}, respectively, for ITP-64, and 1904 and 2003 μmol kg^{-1}, respectively, for ITP-65. A constant A_T was then used essentially removing all DIC variability due to water mass changes within the model. The DIC was incremented at each time step for contributions from air-water gas exchange using the calculated pCO_2. The new pCO_2 was then solved from the A_T, *in situ* temperature and salinity, and the new DIC. This calculation gives the modeled variability of pCO_2 from gas exchange. The remainder of the variability after contribution from gas exchange was assumed to be NCP. A residual least squares approach was used to best fit the DO data. Using this NCP and adjusting for the photosynthetic quotient (1.4), gave a reasonable fit to the pCO_2 data. Since the program calculated the carbonate equilibra and solubility constants as a function of temperature, the effects of heating and cooling on the pCO_2 are intrinsic in the model. A similar approach was used in the DO model. Because DO exists in only one dissolved from, the modeling of DO was comparatively simple. Both pCO_2 and DO gas exchange models were calculated assuming ice-free conditions as well with the goal to show to what extent AO ice coverage controls pCO_2 and DO variability.

2.6.5.3. Photosynthetic model

Net primary production (NPP) was calculated with an exponential model (Platt *et al.*, 1980, Cullen *et al.*, 1992) that takes into account the light (PAR) and Chl-*a* dependence of photosynthesis:

$$NPP = [\text{Chl-}a\ (P_sChl^{-1})(1 - e^{-a})]\ \theta_P^{(T-20)} \qquad (2.15)$$

where NPP is in mg C m^{-3} h^{-1} (C is carbon), Chl-*a* is the concentration of chlorophyll-*a* in mg m^{-3}, P_sChl^{-1} is the Chl-*a*–specific maximum rate of photosynthesis in the absence of photoin-

hibition (mg C mg Chl-a^{-1} hr^{-1}), T is the *in situ* temperature in °C, θ_P is the Arrhenius temperature coefficient (1.036) and

$$a = (\alpha Q_{PAR} (P_s\, Chl^{-1})^{-1})^{-1} \qquad (2.16)$$

where α is the Chl-*a* specific rate of light-limited photosynthesis (in mg C mg Chl-a^{-1} hr^{-1} (μmol quanta m^{-2} s^{-1})$^{-1}$), and Q_{PAR} is the downwelling PAR (in μmol quanta m^{-2} s^{-1}).

Community respiration (R_1) was estimated using the formula below:

$$R_1 = R\, \theta_R^{(T-20)} \qquad (2.17)$$

where R is the nighttime respiration rate based on DO, θ_R is the Arrhenius temperature coefficient (1.045), and T is the *in situ* temperature in °C. We observed that, with a fixed respiration rate, respiration was significantly overestimated over the time-series as the production decreased with decreasing sunlight. Respiration in the dark Arctic is very small (Sherr and Sherr, 2003), therefore, it was assumed to be proportional to NPP where the daily mean of respiration is equal to the mean of NPP on that day, tightly linking NPP and respiration as expected in nutrient-depleted surface waters (Dugdale and Goering, 1967). The new respiration is:

$$R_2 = R_1 \times (NPP \times k) \qquad (2.18)$$

where k is a proportionality constant (0.4) obtained by a residual sum of squares fit. NCP was then calculated as the difference between NPP and R_2.

Chapter 3

Results

The 49-day time-series data for ITP-64 and 41-day time-series data for ITP-65 are shown in Fig. 3.1. Gaps in the data correspond to instrument data communication dropouts between the SAMI and inductive modem. Corresponding physical data are shown in Fig. 3.2. The ice cover near ITP-64 ranged from 0 to 32% with a mean of 10 ± 10%, and ITP-65 ice cover ranged from 38.4 to 89.2% with a mean of 63.2 ± 15.8% (Fig. 3.1e, Table 3.0). Over the deployment time periods, the pCO_2 was well below atmospheric saturation and very similar for both locations. ITP-64 pCO_2 ranged from 282 to 323 μatm with a mean of 306 ± 9 μatm, and ITP-65 from 272 to 330 μatm with a mean of 304 ± 16 μatm (Fig. 3.1a, Table 3.0). ITP-64 pCO_2 steadily increased from ~285 to 310 μatm until around 09/23/12 when it leveled off (Fig. 3.1a). DO showed very little variability at both locations but were above or near saturation for the most of the time period (Fig. 3.1b, saturation is not shown. The saturation level ranged between 100.8 and 105.2% with the mean being 102.8 ± 1% for ITP-64, and between 99.2 and 103.3% with the mean being 101.3 ±1% for ITP-65). ITP-64 DO ranged from 387 to 395 μmol kg^{-1} with a mean of 392 ± 2 μmol kg^{-1} and ITP-65 from 381 to 390.3 μmol kg^{-1} with a mean of 385 ± 2 μmol kg^{-1} (Fig. 3.1b, Table 3.0). DO levels were above or near saturation for the most of the time period. The diurnal cycles are distinct in ITP-64 DO data (Fig. 3.1b) until the daylight period approached zero around 10/06/12 (Fig. 4.3), whereas in ITP-65 DO data they are almost absent (Fig. 3.1b). Diurnal cycles in DIC at ITP-64 are also evident once the long-term trend is removed (see below).

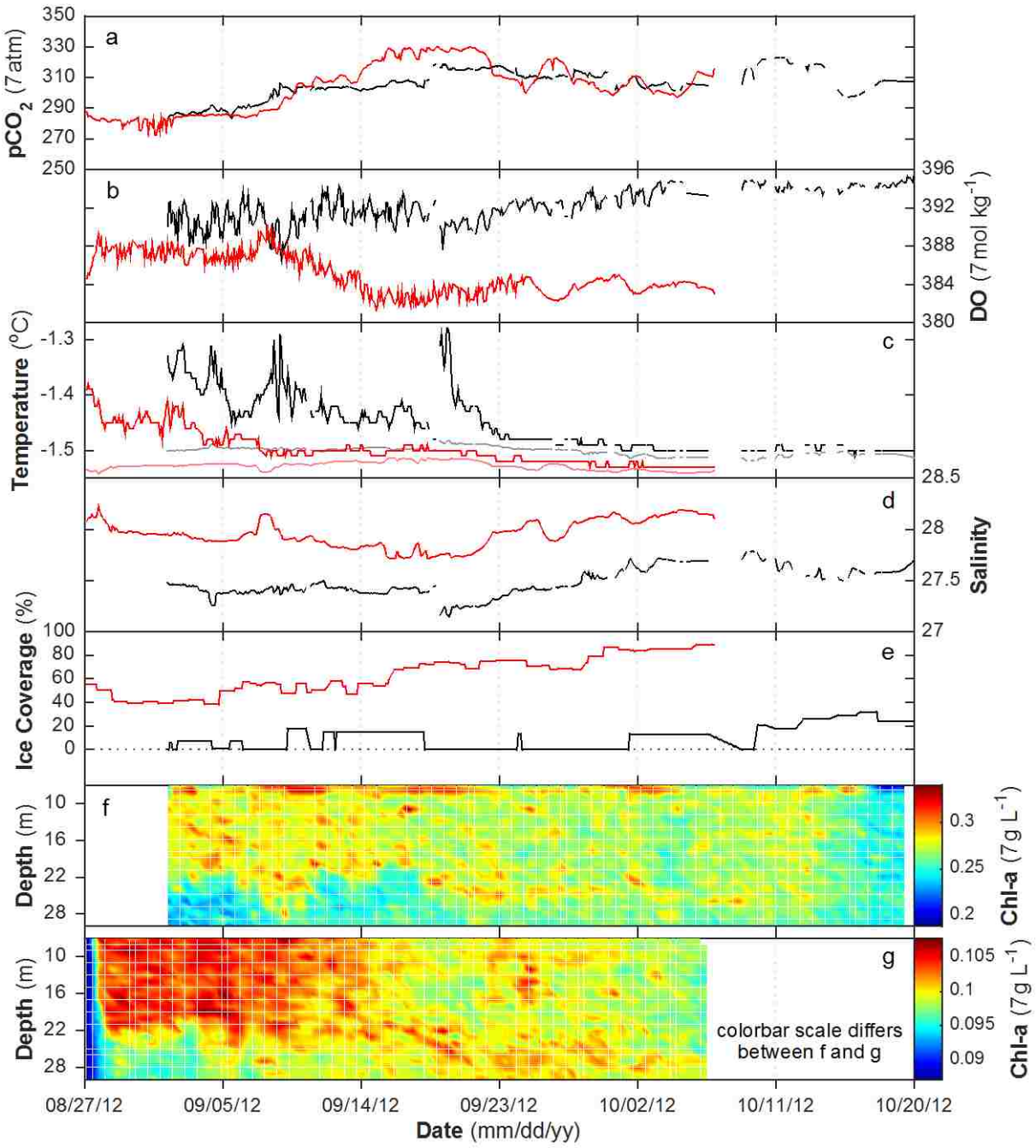

Figure 3.1. Biogeochemical and physical time-series data collected at ~6 m on ITP-64 (black) and ITP-65 (red) (panels a-d). ITP-64 was deployed under little ice whereas ITP-65 was deployed under multi-year ice (panel e). Gaps in the data correspond to instrument communication dropouts. The light black line and light red line in the temperature plot refer to freezing temperature of water at ITP-64 and ITP-65, respectively (panel d). Note that the colorbar scale changes from panel f to g.

ITP-64 temperature was slightly higher than ITP-65 temperature until they converged towards the freezing point (Fig. 3.1c). The freezing point of seawater was ~0.03 °C higher at ITP-65 due to the significantly higher salinity. ITP-65 approached freezing temperature around 09/21/12, a couple of days earlier than ITP-64 (Fig. 3.1c). The difference in salinity between the two ITPs locations was relatively large considering the distance between the locations. ITP-64 salinity had a mean value of 27.5 ± 0.1, whereas ITP-65 had a mean value of 28.0 ± 0.1 (Fig. 3.1d, Table 3.0). Over most of the measurement period, ITP-64 Chl-*a* was ~3 times higher than ITP-65 Chl-*a* (Fig. 3.1f, 3.1g; Table 3.0). The atmospheric pCO_2 measured in Barrow, Alaska ranged from 375.4 to 404.8 μatm with a mean of 385.6 ± 5.8 μatm. The average depth of mixed layer was 21.5 ± 2.0 m at ITP-64 and 22.0 ± 2.5 at ITP-65 (Fig. 3.2).

Table 3.0 The mean ± standard deviation of the difference for different parameters for ITP-64 and ITP-65 at ~6 m depth. The right-most column includes the difference between the mean of the parameters.

Parameters	**ITP-64**	**ITP-65**	**Mean Difference** (ITP-64 - ITP-65)
Ice coverage (%)	10 ± 10	63.2 ± 15.8	-53.2
Temperature (°C)	-1.46 ± 0.05	-1.50 ± 0.03	0.04
Salinity	27.5 ± 0.1	28.0 ± 0.1	-0.5
*p*CO2 (μatm)	306 ± 9	304 ± 16	2.4
Δ*p*CO2 (μatm)	-79.5 ± 9.5	-80 ± 15	-0.5
CO2 flux (mmol m^{-2} d^{-1})	-7.8 ± 6.8	-2.5 ± 2.6	5.3
DO (μmol kg^{-1})	392 ± 2	385 ± 2	7.4
ΔDO (% saturation)	3.0 ± 0.1	1.3 ± 0.1	1.7
DO flux (mmol m^{-2} d^{-1})	15.6 ± 12.6	2.2 ± 2.7	13.4
Chl-*a* (μg L^{-1})	0.28 ± 0.01	0.100 ± 0.002	0.18
NCP (mmol m^{-2} d^{-1})	7.4	~0	7.4
GPP (mmol m^{-2} d^{-1})	13	~0	13

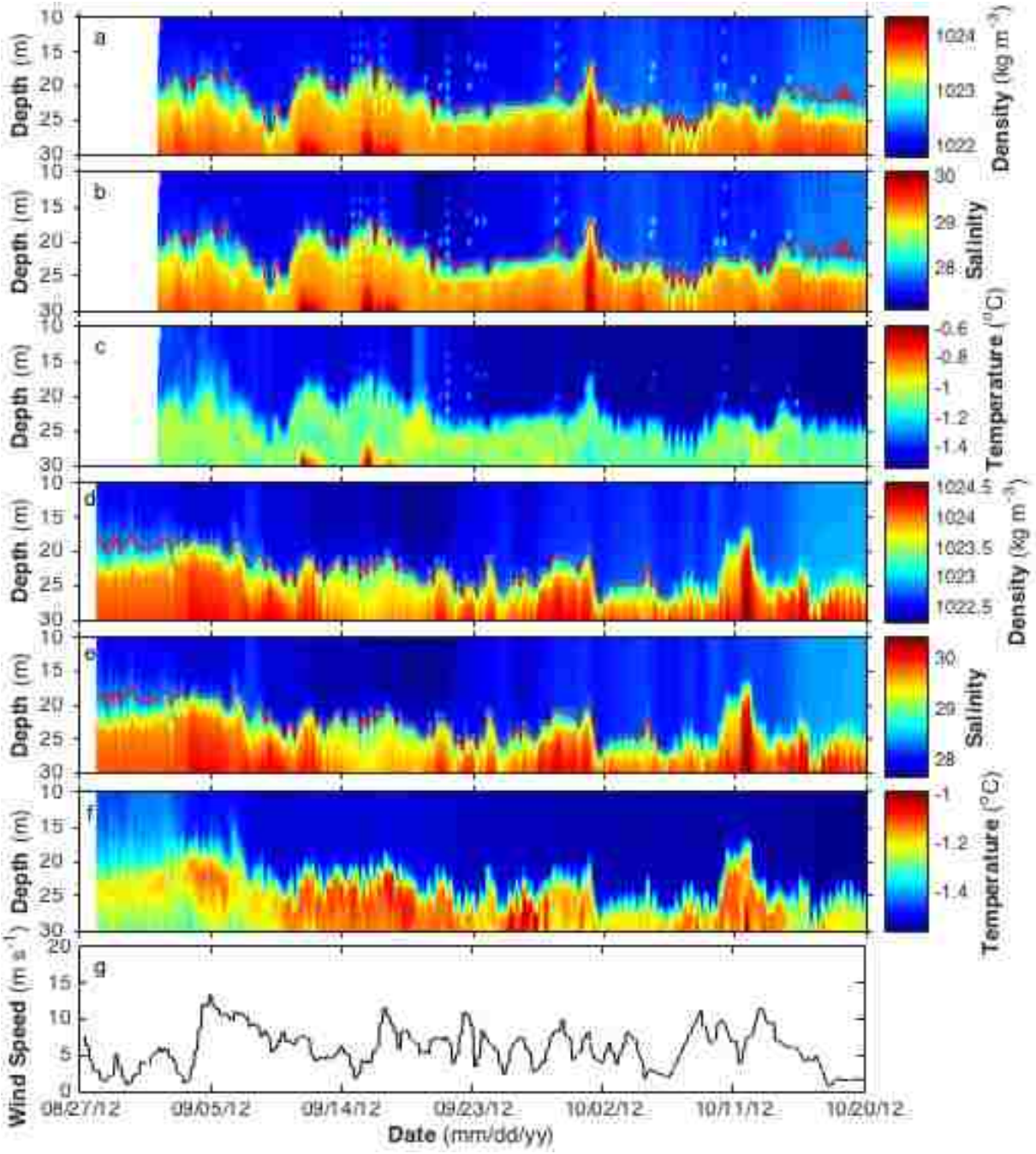

Figure 3.2. Depth-resolved density, salinity and temperature contour plots for ITP-64 are shown in panel a, b and c, respectively, and those for ITP-65 are shown in panel d, e and f, respectively. MLDs (red line) are overlapped on the density (panels a and d) and salinity (panels b and e) contour plots. Wind speed is shown in panel e. Wind speed was uniform over both locations.

Chapter 4

Discussion

4.1. Observations based on *in situ* data and model estimates

The variability of CO_2 and DO was investigated based on various processes that contribute to the variability as described by Equation 2.12. Partially open-water and partially ice-covered *in situ* biogeochemical data are shown in Fig. 3.1. Biogeochemical models were employed to better explain the potential contribution from the major processes (Fig. 4.1, 4.5 and 4.6). We examine the contribution from gas exchange to the variability of CO_2 and DO in seawater under *in situ* ice cover and assuming ice-free condition, and then investigate the contribution of NCP to the variability. Other possible mechanisms that may have influence on the variability have also been assessed.

4.1.1. ITP-64

Results from biogeochemical models are compared with *in situ* pCO_2 and DO data in Fig. 4.1. The models reproduced the major features and overall long-term trends in pCO_2 and DO variability reasonably well. The model pCO_2 trend due to gas exchange initially matches the *in situ* data (r^2=0.92), but overshoots after 9/23/12 (Fig. 4.1a). *In situ* pCO_2 maintained significant correlation with CO_2 gas flux (r^2=0.75), which dropped dramatically after 09/23/12 (r^2=0.08). The modeled gas exchange with no ice is very similar (Fig. 4.1) because there is very little ice coverage at this location (Fig. 3.1e). The DO model from gas exchange should in principle follow the DO data until 09/23/12 as with pCO_2, which it did not (Fig 4.1b). The DO maintained very weak correlation with pCO_2 until 09/23/12 (r^2=0.001). This may be attributed to the relative saturation levels between pCO_2 and DO (26% pCO_2 and 3% DO) that

make the CO_2 gas exchange more dominant, and makes DO not correlate strongly with gas exchange. The correlation between pCO_2 and DO becomes stronger after 09/23/12 (r^2=0.60) as phytoplankton production, though small later, continued to add DO to seawater and gradual increase in sea ice cover (Fig. 3.1e) resulted in accumulation of DO in water due to reduced sea to air flux of DO. Gas exchange drives modeled DO quickly to saturation and under predicts observed DO levels (Fig. 4.1b). These deviations from the *in situ* data indicate that there are some other process decreasing pCO_2 and increasing DO, counteracting the air-sea exchange.

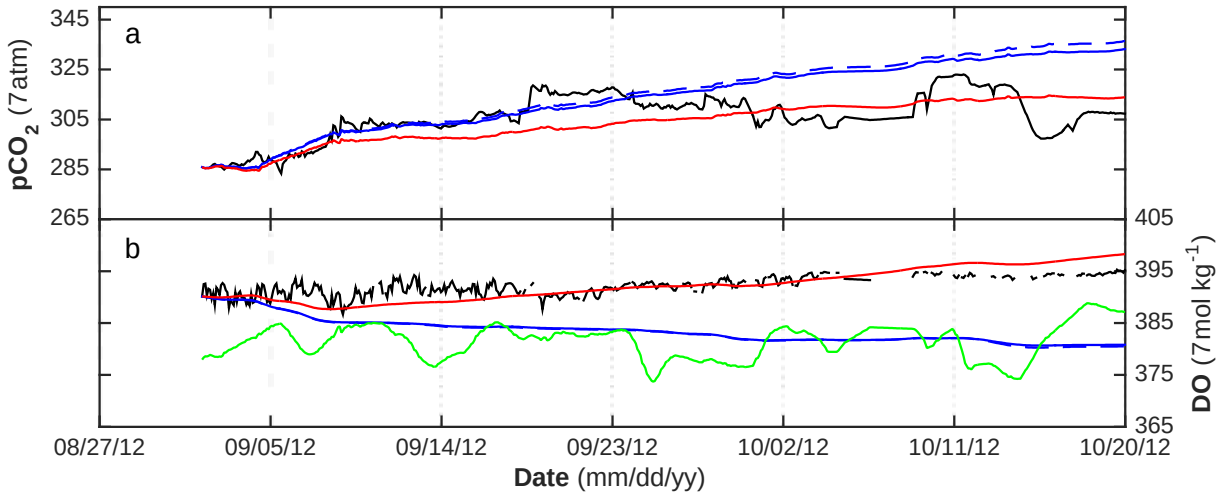

Figure 4.1. ITP-64 pCO_2 and DO data (black) and model time-series data calculated from modeled gas exchange using the ice cover (blue solid) shown in Fig. 3.1 and without ice cover (blue dashed). Modeled gas exchange plus NCP assuming the residual signal is all NCP are shown (red). The green line corresponds to the equilibrium concentration of O_2 at *in situ* temperature, salinity and atmospheric pressure.

If the remainder of the variability is assumed to be NCP, a residual least squares approach finds an NCP of 8.6 mmol DO m^{-2} d^{-1} to best fit the ITP-64 DO data (r^2=0.60) (Fig. 4.1b, red curve). Using this NCP and adjusting for the photosynthetic quotient (1.4) gives a reasonable fit to the pCO_2 data (r^2=0.55) (Fig. 4.1a). These results suggest that biological production is an important contributor to pCO_2 and DO variability in this low ice-coverage gas record. This speculation is supported by the significant levels of Chl-*a* (Fig. 3.1f) and that there were detectable nutrients. The nitrate concentration in the ITP-64 mixed layer varied between 0.2 and 2 μM (Fig. 4.2). If all of these nutrients were utilized by photosynthesis, DIC at ITP-64 would go down by ~7 μmol kg^{-1} and DO would go up by ~10 μmol kg^{-1} based on Redfield stoichiometric calculations (Redfield, 1934) (Equation 4.1), manifesting the significant influence of nutrient-fueled biological activity on the variability of pCO_2 and DO at that location. According to the residual fit model, DIC at ITP-64 went down by 19 μmol kg^{-1} and DO went up by 18 μmol kg^{-1} due to NCP. The Redfield stoichiometric equation is:

$$C:N:P = 106:16:1 \qquad (4.1)$$

where C is carbon, N is nitrogen, and P is phosphorous.

The NCP derived by the best-fit approach is close to the daily mean NCP, 7.4 mmol DO m^{-2} d^{-1} and 7.0 mmol C m^{-2} d^{-1} (C = CO_2), calculated from the bandpass filtered DO and DIC data (Fig. 4.4b). As can be seen in Figure 4.3, the filtered data more clearly show the diurnal pattern in the DO and CO_2 data. The NCP from DIC matches with the NCP from DO during some periods (e.g. r^2=0.72 from 09/04/12 to 09/07/12), however, at times they are poorly correlated. These times of poor correlation correspond to periods when salinity rapidly changed (marked by arrows in Fig. 4.4a) suggesting lateral advection of different water masses. The decoupling (non-Redfield variability) of CO_2 and DO may be due to advection of a

residual production signal where, for example, a bloom has occurred in the past. The DO more rapidly equilibrates with the surface ocean leaving behind a residual CO_2 signal (DeGrandpre *et al.*, 1998). When water masses moved by the sensors, the DO did not vary as much as the pCO_2 (or DIC). These appear as large oscillations in the NCP calculated from DIC (Fig. 4.4b).

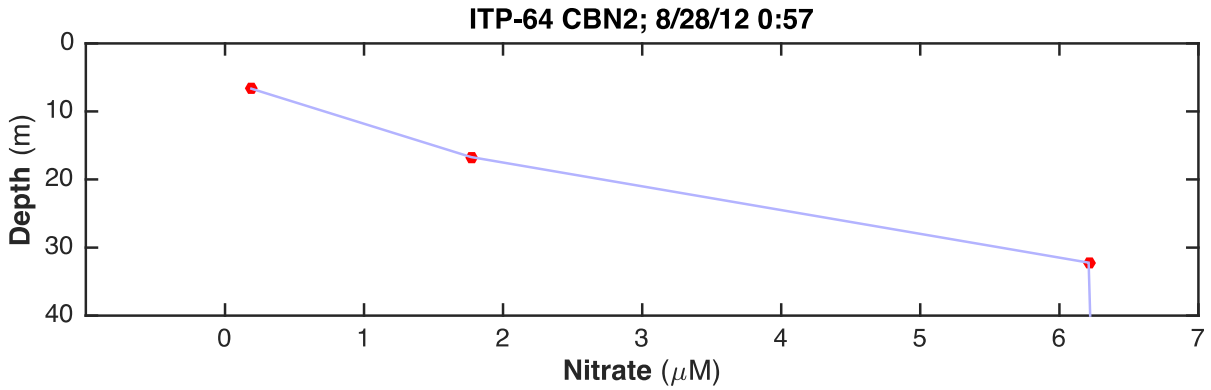

Figure 4.2. Nitrate concentration (red dot) in the mixed layer sampled at station CBN2 near ITP-64. The date and time for the first sampling are included on top of the figure. The samplings were done at 3 minute intervals. The average MLD at ITP-64 is 21.5 ± 2 m.

The photosynthetic model that calculated NCP using Chl-*a* and PAR data (Equation 2.15, Fig. 4.3) found a mean NCP of 7.2 mmol C m^{-2} d^{-1}. The modeled data was compared with bandpass filtered NCP data calculated from *in situ* DO and it reproduced the rate of change in DO in seawater considerably well (r^2=0.70) (Fig. 4.3), suggesting that the daily rate of change in DO in seawater was for the most part driven by biological activity i.e. photosynthesis. The model used an α value of 0.04 mg C mg Chl-a^{-1} hr^{-1} (μmol quanta m^{-2} s^{-1})$^{-1}$, which is the initial slope of the photosynthesis rate per unit water column and the instantaneous PAR intensity relationship. The P_sChl value used in the model was 33 mg C mg Chl-a^{-1} hr^{-1}, based on residual fit. Average nighttime respiration based on the rate of change in DO was 34 mmol m^{-2} d^{-1}.

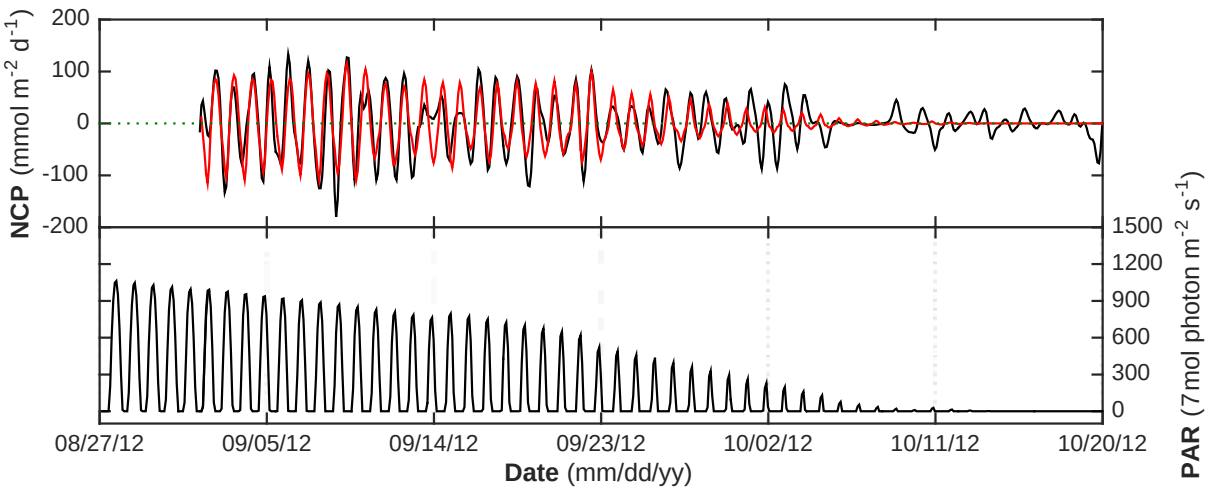

Figure 4.3. ITP-64 modeled NCP calculated from Chl-*a* and PAR (red), and NCP calculated from *in situ* bandpass filtered DO (black, same data as shown in Figure 4.3). The model reproduces photosynthesis-driven rate of change in DO in seawater reasonably well (r^2=0.70). After 09/26/12, NCP from DO was significantly influenced by other (mostly advection) processes and modeled NCP became smaller and smaller as the length of daytime approached zero (PAR, lower figure). This model was not employed for ITP-65, as NCP was negligible based on the DO model results (see text). The PAR data shown here corresponds to solar radiation at ~8 m depth, which was initially scaled using the surface PAR data collected on the ship.

Although air-sea gas exchange and NCP explained pCO_2 and DO variability reasonably well and advection seemed to have significantly influenced the variability, there is some variability in the data that could not be explained, especially in the CO_2 record (Fig. 4.1). This variability may be linked to water movement. Timmermans *et al.* (2012) found that the ocean surface layer beneath sea ice in the Canada Basin is characterized by significant horizontal density gradients and concluded that submesoscale (a scale of intermediate size) processes significantly influence lateral density variability and the properties of the surface-layer. The surface waters in the central basin have distinctly different physical and chemical properties compared to the subsurface halocline, influencing the inventory of DIC and DO in the mixed layer. This is what likely created the large swings in the calculated NCP, as explained above.

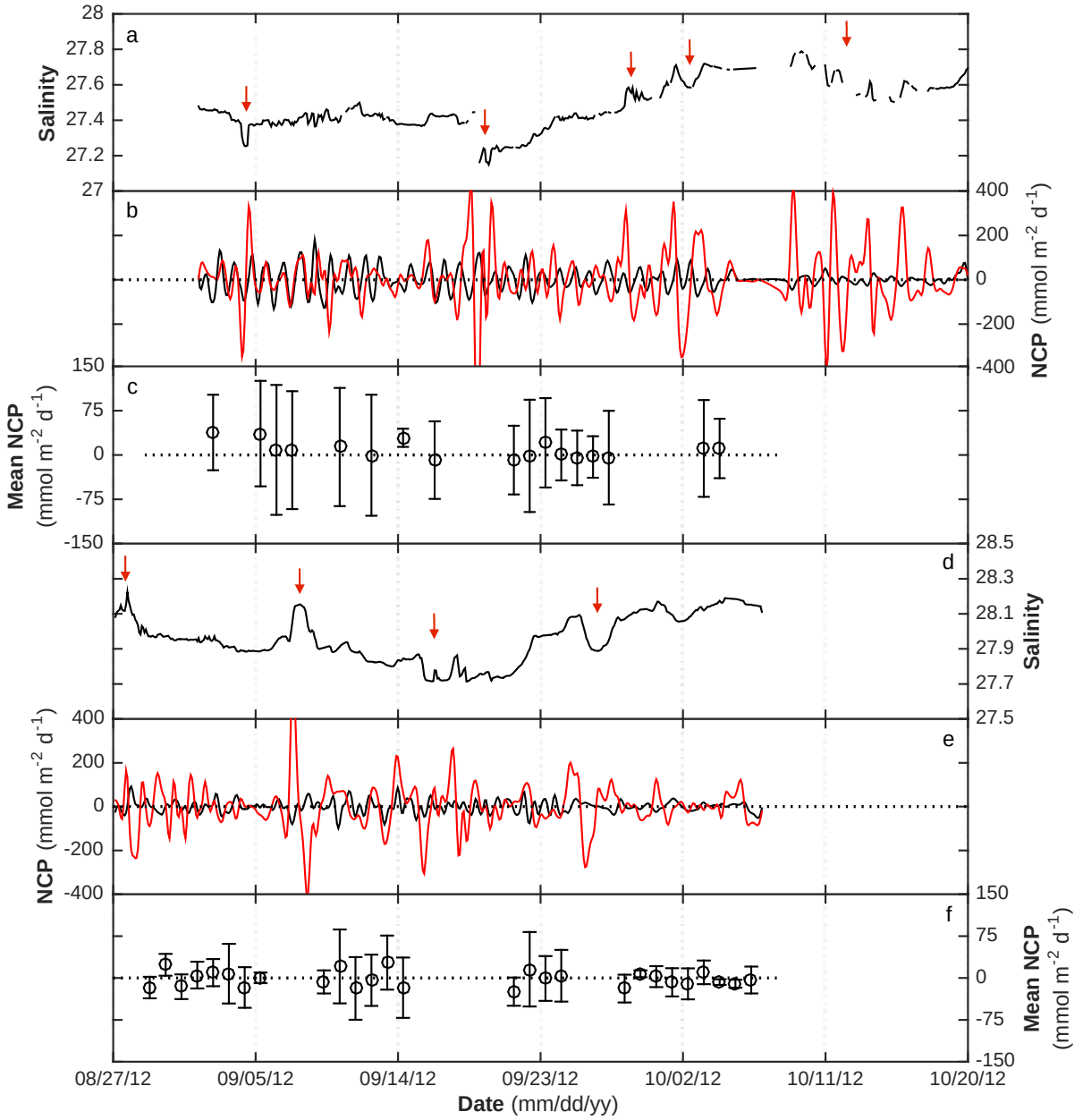

Figure 4.4. ITP-64 salinity and biogeochemical data are shown in panel a-c and ITP-65 data are shown in panel d-f where NCP from DIC and DO are shown in red black, respectively. Abrupt changes in salinity data highlighted by downward arrow in panel a and d indicate potential advection of waters with different levels of pCO_2 and DO, thereby this short-term variability appears in the NCP calculated from the rate of change in DO (black) and DIC (red), shown in in panel b and e. NCP from DO is compared with NCP from DIC after conversion with photosynthetic quotient (1.4). Daily mean (circle) ± standard deviation (vertical bars) of NCP calculated from DO are shown in panel c for ITP-64 and f for ITP-65. The mean was calculated over a 24 hour period starting at 8 a.m.

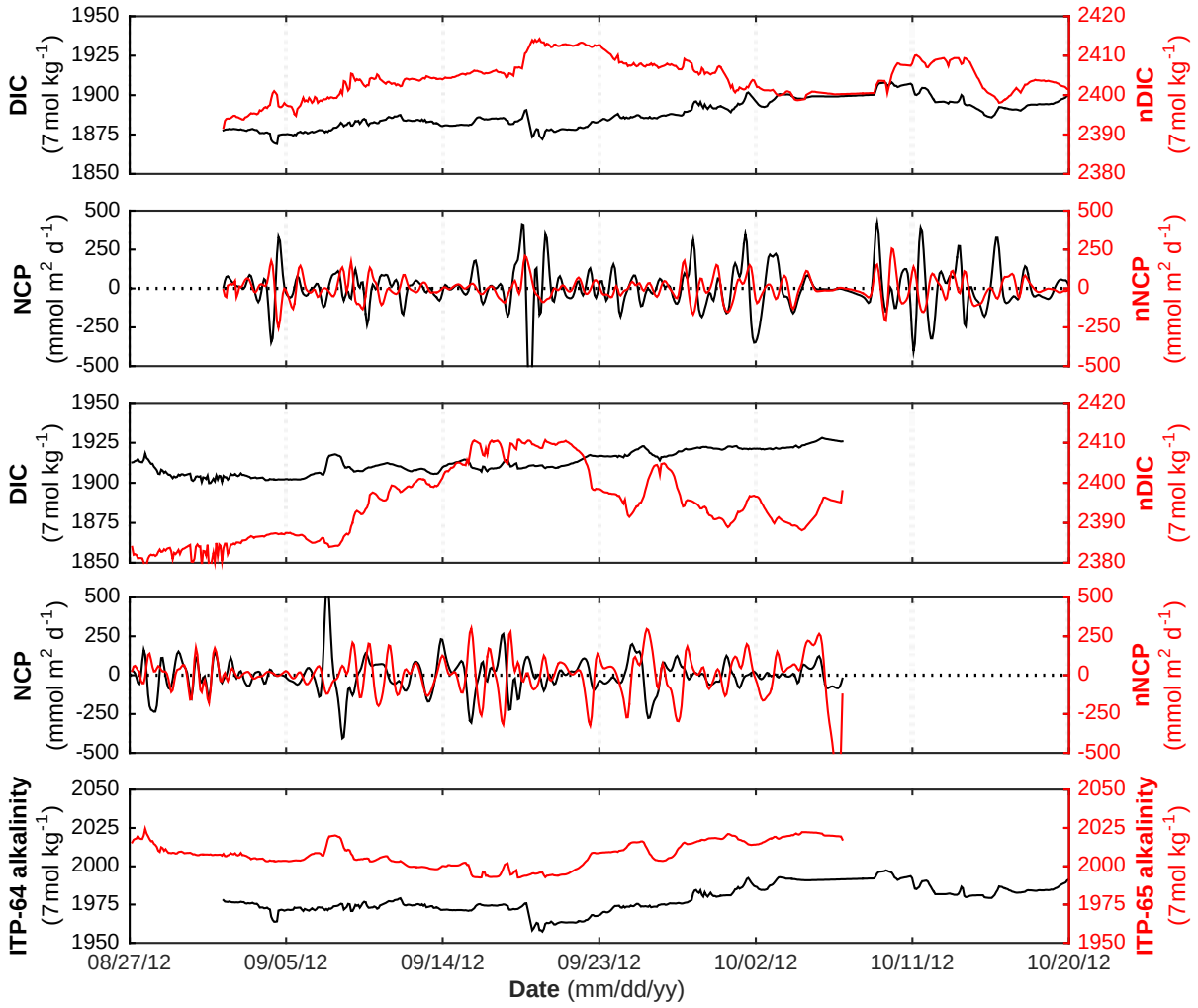

Figure 4.5. Comparison between *in situ* DIC (black) and normalized DIC (red) for ITP-64 and ITP-65 are included in panel a and panel d, respectively. NCP calculated from DIC (black) are compared with NCP calculated from normalized DIC (red) in panel b and panel d, which correspond to ITP-64 and ITP-65, respectively. Normalized data differ considerably from the parent data suggesting that the influence of local and non-local process is significant at both ITP locations.

Others have observed that brine formation can be a significant contributor to mixed-layer and pycnocline DIC and DO levels (Nomura *et al.*, 2006; Rysgaard *et al.*, 2007). Ice formation could have occurred after ~09/23/12 based on the temperature. However, if F_{brine} was significant DO and pCO_2 would simultaneously go up as the gases are rejected from the ice, which they did not (Fig. 4.1), indicating that brine formation was not a significant factor. All of these observations point to the conclusion that, apart from gas exchange and NCP, horizontal gradients was the only other process to significantly contribute to the pCO_2 variability, whereas DO variability for the most part was dominated by gas exchange and NCP.

4.1.2. ITP-65

We compared *in situ* pCO_2 and DO to modeled pCO_2 and DO calculated from gas exchange (Fig. 4.6) for data from ITP-65. The model initially fits the pCO_2 trend reasonably well (r^2=0.60 until 09/09/12) but does not fit well where there are humps in the *in situ* pCO_2 data (e.g. around 09/10/12, 09/26/12, 10/02/12). pCO_2 increased until 09/15/12 (Fig. 4.6a), then leveled off until 09/22/12, after when it varied up and down around a mean of ~315 μatm until the end of the measurement period. On the other hand, gas exchange explains almost all of the DO variability (Fig. 4.6b). The correlation coefficient between *in situ* DO and DO modeled from gas exchange is 0.53, which becomes 0.82 when the sudden changes around 09/08/12, 09/26/12 and 10/02/12 are ignored. DO maintained a mean of ~388 μmol kg^{-1} until 09/06/12 (Fig. 4.6b), after this date it steadily went down to ~384 μmol kg^{-1} and maintained this mean value until 09/23/12. After 09/23/12, DO varied up and down around the mean of ~384 μmol kg^{-1} until the end of the measurement period. Based on the model, gas exchange keeps the DO near saturation. However, the contribution from gas exchange to the variability of pCO_2 and DO under heavy ice cover is small relative to that if no ice is present (Fig. 4.6).

Rutgers van der Loeff *et al.* (2014) found that gas transfer velocity in the ice-covered central AO regions is small (<0.42 cm hr^{-1}) when a residence time of at least 200 days is given. Therefore, CO_2 and O_2 exchange through ~63% ice cover at ITP-65 can be assumed small, which it is. pCO_2 levels in seawater increase by 21.13 µatm, whereas DO decreases by 3.08 µmol kg^{-1} when ice-free condition is assumed (Fig. 4.6), manifesting that ice cover significantly inhibits gas exchange.

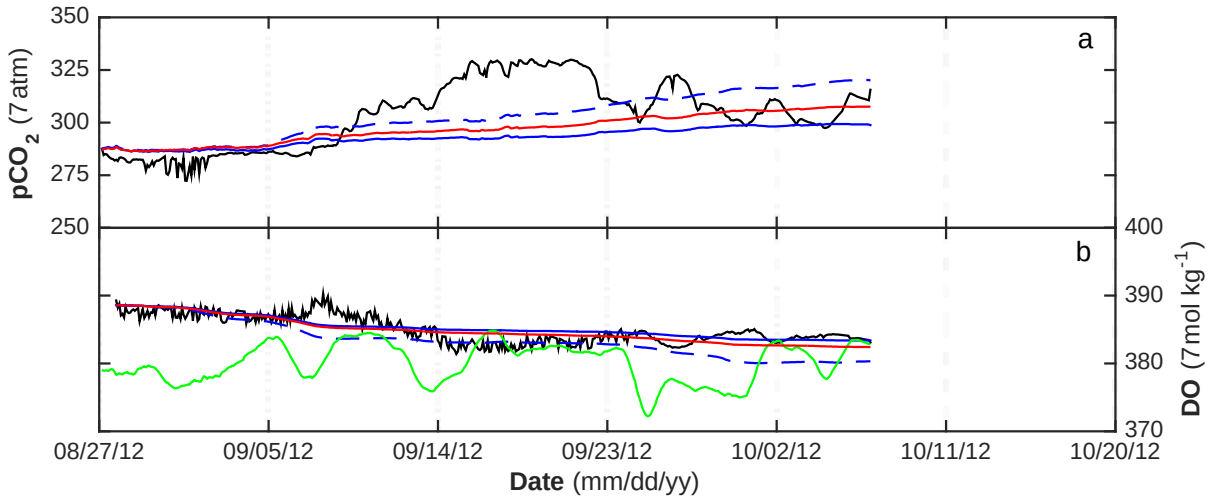

Figure 4.6. ITP-65 pCO_2 and DO data (black) and model time-series data calculated from modeled gas exchange using the ice cover (blue solid) shown in Fig. 3.1 and without ice cover (blue dashed). Modeled gas exchange plus NCP assuming the residual signal is all NCP are shown (red). Green lines correspond to the equilibrium concentration of O_2 at *in situ* temperature, salinity and atmospheric pressure.

The DO results based on gas exchange support that other sources of variability such as NCP, brine formation and vertical mixing are negligible. NCP is low as light under multiyear ice is too small and nutrients are too depleted (Fig. 4.7) to sustain significant production. NCP is low as it is primarily light-limited and availability of light under multiyear ice is too small to sustain significant production. There was no detectable nitrate in the ITP-65 mixed layer and Chl-*a* was small, almost 3 times smaller than ITP-64 Chl-*a*. Although DO variabil-

ity for the most part can be explained by gas exchange, there are some big changes in pCO_2 (around 09/10/12, 09/26/12, 10/02/12; Fig. 4.6a) that gas exchange, NCP (NCP ~0), F_{brine} could not explain. These changes are potentially linked to horizontal advection, as discussed in the case of ITP-64. These influences can be observed in the salinity data (highlighted by downward arrow, Fig. 4.4d), which suggests episodic mixing of water masses with different salinities (e.g. around 09/08/12, 09/26/12, 10/02/12). These observations indicate that horizontal gradients significantly dominated the pCO_2 variability under multiyear ice, whereas DO variability for the most part was dominated by gas exchange.

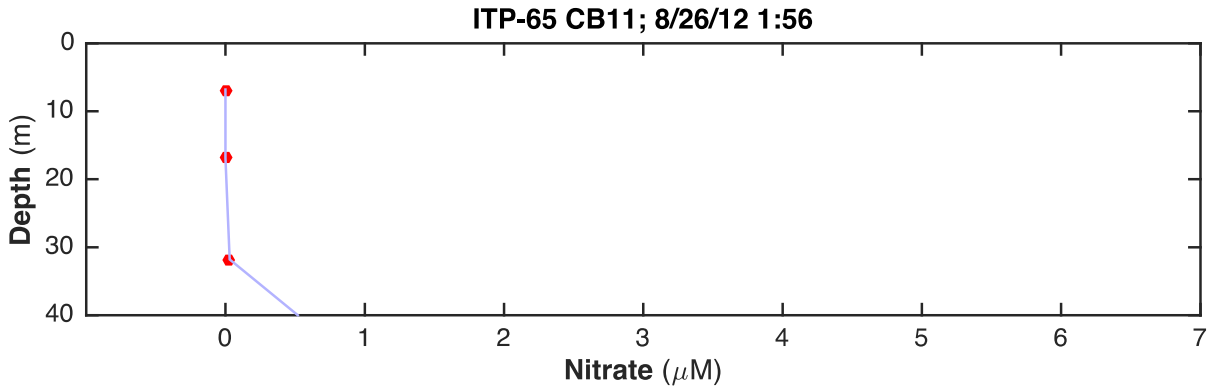

Figure 4.7. Nitrate concentration in the ITP-65 mixed layer. The date and time for the first sampling are included on top of the figure. Samplings were done at 3 minute intervals. The average MLD at ITP-65 is 22.0 ± 2.5 m.

4.2. Air-sea fluxes of CO_2

We compared our CO_2 flux estimates with previous estimates from the Canada Basin and nearby regions. Our estimated CO_2 flux during late summer-autumn is -7.8 ± 6.8 mmol m^{-2} d^{-1} for ITP-64 and -2.5 ± 2.6 mmol m^{-2} d^{-1} for ITP-65 (Fig. 4.8, Table 3.0). The range of variability at each site is primarily dominated by the gas transfer velocity (Equation 2.14) because of the highly variable wind speed (Fig. 4.8). Murata and Takizawa (2003) found that the

CO_2 flux in the slope waters of western AO during the summers of 1998-2000 ranged between −16.9 and −0.1 mmol m^{-2} d^{-1} and was -12 mmol m^{-2} d^{-1} in the western Beaufort Sea. In the spring of 2002 and 2004, Bates *et al.* (2006) estimated < -3 mmol m^{-2} d^{-1} CO_2 flux in the Canada Basin, when sea-ice cover ranged from 95% to 100%. During summertime, the fluxes in the Canada Basin were higher at ~ −55 mmol m^{-2} d^{-1}, when sea-ice cover ranged from 0% to 90%. Our CO_2 flux estimates over the entire summer period (assuming 90 days of period when ice coverage is less) are -0.70 mol m^{-2} for ITP-64 and -0.23 mol m^{-2} for ITP-65. Since air-sea gas flux in the Canada Basin is expected to be virtually negligible for the most of the year due to significant ice-cover, we assume that our late summer-autumn flux values are reasonable estimates of annual CO_2 flux in the region. When the flux estimates are extrapolated over the entire Canada Basin with an area of 4,489,000 km^2 (Macdonald *et al.*, 2009), the CO_2 flux is estimated to be -21.5 Tg C yr^{-1} (Tg = teragrams = 10^{12} grams) under ITP-64 condition (10 ± 10% ice cover) and -6.5 Tg C yr^{-1} under ITP-65 condition (63 ± 16% ice cover). Bates *et al.* (2006) estimated the annual CO_2 flux in the Canada basin to be in the range of -6 to -19 Tg C yr^{-1}, appreciably close to our range. When the entire AO area of 10,700,000 km^2 (Macdonald *et al.*, 2009) is considered, our flux estimates are -51.4 Tg C yr^{-1} and -15.4 Tg C yr^{-1} under ITP-64 and ITP-65 conditions, respectively. In comparison, annual flux estimates over the AO as reported by Anderson *et al.* (1994) (mass balance assessment), Lundberg and Haugen (1996) (mass balance assessment, includes Norwegian Sea), Anderson *et al.* (1998) (mass balance assessment), Anderson *et al.* (1998) (mass balance assessment, includes river contribution), Kaltin and Anderson (2005) (mass balance assessment), Bates (2006) are -70 ± 65, -110, -24 ± 17, −41 ± 18, -31, and -66 Tg C yr^{-1}, respectively. Our fluxes at ITP-64 are similar to those estimated by Evans *et al.* (2015) from shipboard pCO_2 data for

the western Arctic coastal ocean calculated from flux climatologies with the 2003 and 2014 sea ice, and 2003-2014 sea ice climatology.

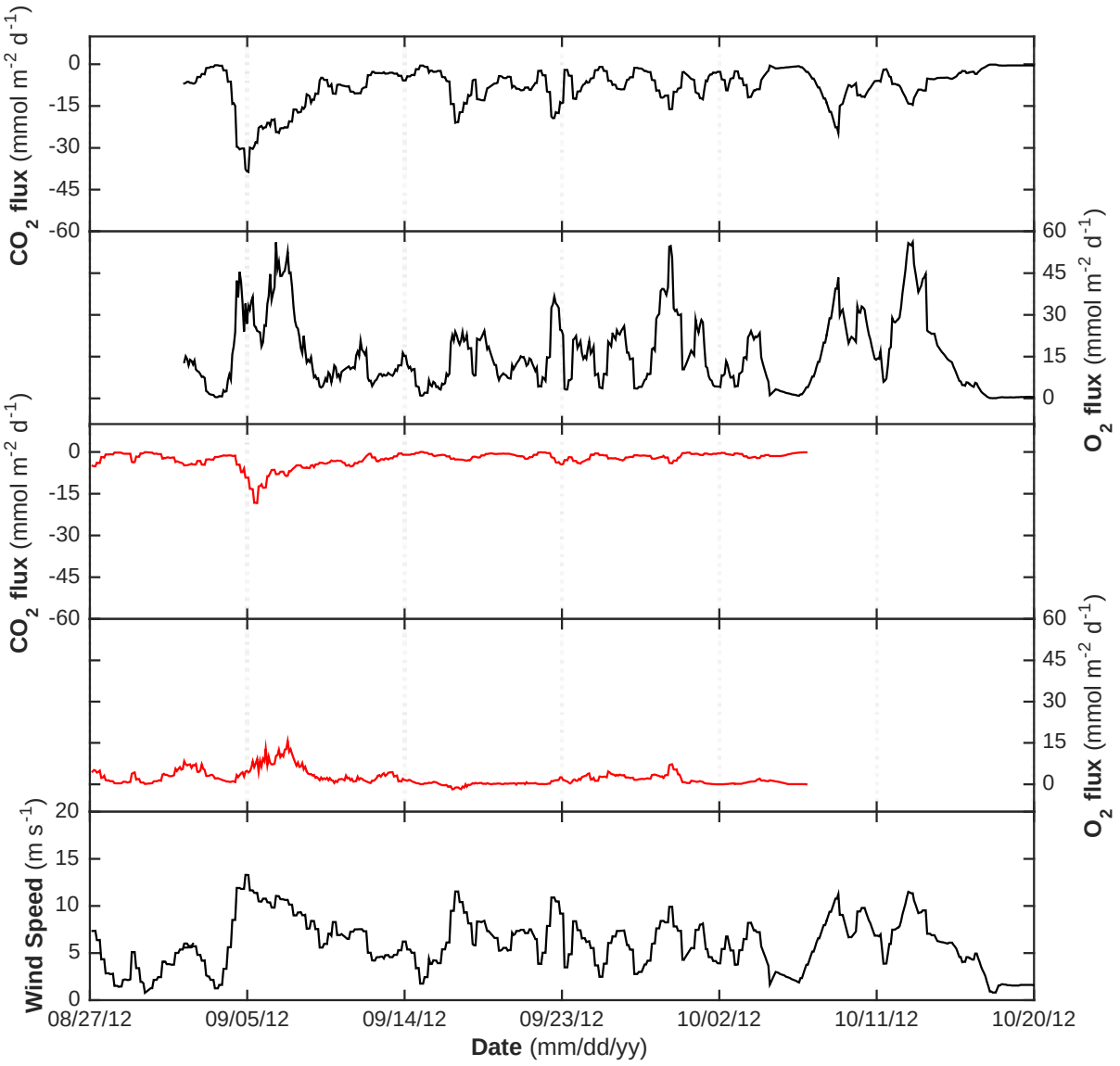

Figure 4.8. CO_2 and O_2 gas flux across air-sea interface are shown for ITP-64 (black) and ITP-65 (red). Negative flux means air to sea gas transfer and vice versa. Fluxes for ITP-65 are considerably smaller than ITP-64 due to heavy ice coverage. The wind speed was uniform over both locations.

Our estimates and all these data show that CO_2 flux in the central AO is considerably variable in space and time. As a strong storm hit the Arctic in the early August of 2012, we compared the wind speed during our study to previous data to see how it compares to typical wind at the Canada Basin and if the post-storm period had a significant influence on our CO_2 gas flux estimate. During our measurement period, the wind speed ranged from 0.8 to 13.3 m s^{-1} with the mean being 6.2 ± 2.7 m s^{-1} (Fig. 4.8). According to NCEP reanalysis data, the average wind speed during 1992-2009 at the Canada Basin stayed fairly constant at about 5 m s^{-1} during winter months October to January (JRA, ERA-Interim, and NCEP-2 ≥6 m s^{-1}), which reduced towards spring and summer (Spreen *et al.*, 2011). During 2005-2006 (a winter storm hit in the winter of 2005-06) and 2007-2008, the strongest wind speed had a maximum daily average of over 14 m s^{-1} and 10 m s^{-1}, respectively, with a daily average of about 10 m s^{-1} during 2005-2010 time period (Jackson *et al.*, 2012). The upper limit of the range of the wind speed during our measurement resembling that in 2005-2008 strong wind periods suggests that the wind during our study was strong and likely an aftermath of the storm that hit in the early August, and may have had significant influence on CO_2 gas flux, making the conditions different from many previous studies.

4.3. NCP

The annual or seasonal average NCP in the deep central AO basins are generally low compared to the adjacent shelf seas (Anderson *et al.*, 2003; Codispoti *et al.*, 2013; Sakshaug, 2004) or other open water regions, due primarily to insufficient availability of light and nutrients (Popova *et al.*, 2010; Sakshaug, 2004; Vancoppenolle *et al.*, 2013). This situation is unlikely to change much unless nutrients from 50 m or greater depths can be made available for phytoplankton growth (Codispoti *et al.*, 2013). Even in a more open-water AO, where produc-

tion is expected to increase due to increased amount of area exposed to light, nutrients may be the more limiting factor for production (Tremblay and Gagnon, 2009). Low NCP and GPP values in the AO basin were found in many previous studies, though few estimates from the deep AO during late summer/early fall have been made so far with most studies focused on the productive marginal seas (e.g., Cross *et al.*, 2012; Shadwick *et al.*, 2011; Wassmann *et al.*, 2006).

We have estimated 7.4 mmol m^{-2} d^{-1} of NCP in the partially ice-covered sea surface water (corresponding to ITP-64) and ~0 mmol m^{-2} d^{-1} under multiyear ice-covered sea surface water (corresponding to ITP-65). Olli *et al.* (2007) estimated primary production in the Amundsen basin (89–88° N) of the central AO during the peak of the productive season (August 2001) to be 4.2-12.5 mmol m^{-2} d^{-1} in a ~15% ice-free surface. In 2002, Bates *et al.* (2005) measured NCP during spring (5 May-15 June) and summer (15 July-25 August) in the Canada Basin to be <1.25-2.08 mmol m^{-2} d^{-1}, with NCP in shelf regions being significantly higher (83-238 mmol m^{-2} d^{-1}). Hill *et al.* (2005) estimated 30 mmol m^{-2} d^{-1} productivity in the euphotic zone on the edge of the Canada Basin during summer 2002. Ulfsbo *et al.* (2014) reported low NCP values (<1 mol m^{-2} over 63 days) in the ice-covered deep AO basins during late summer of 2011 (5 August - 7 October), with a strong spatial variability, but they sampled significantly larger area than ours. Previous studies have reported productivity in the range of 3.75-10.25 mmol m^{-2} d^{-1} in the deep AO (Cota *et al.*, 1996; Wheeler *et al.*, 1996; Gosselin *et al.*, 1997; Chen *et al.*, 2002).

As stated earlier, insufficient availability of light and nutrients limits production in the AO. The nitrate concentration in the ITP-65 mixed layer under heavy ice cover was virtually zero, whereas in the ITP-64 mixed layer it was in a detectable amount (Fig. 4.2, 4.6). The nu-

trients in the ITP-64 mixed layer were potentially a result of previous mixing that occurred due to winds when the surface water was open to the atmosphere. According to the wind speed record, the wind was strong prior to when the nutrients were measured during the ITP deployment (Fig. 4.8). In addition, advective mixing and tidal mixing can also introduce nutrients into the photic zone (Codispoti *et al.*, 2013). The vertical profile of DO and DIC in the mixed layer (Fig. 4.9 and 4.10) may provide information about mixing events. If biological activity dominates the DO and DIC variability in the mixed layer they would maintain a negative relationship. A positive relationship between DO and DIC suggests mixing that brought up both DO and DIC from the deep water, which seems to have happened weakly at ITP-64. Our NCP estimates show that even with open water conditions NCP remained very low in the AO basin (Fig. 4.4b), which is typical of oligotrophic oceans (see Polovina *et al.*, 2008). Although the NCP is considerably low even in the partially open seawater (at ITP-64) it is significantly higher than that in the ice-covered water (at ITP-65) (Fig. 4.4b and 4.4e), suggesting open water sustains higher production compared to ice-covered water. The gross primary production (GPP), calculated as NCP plus respiration, was also estimated and they are 13 mmol m^{-2} d^{-1} at ITP-64 and ~0 mmol m^{-2} d^{-1} at ITP-65.

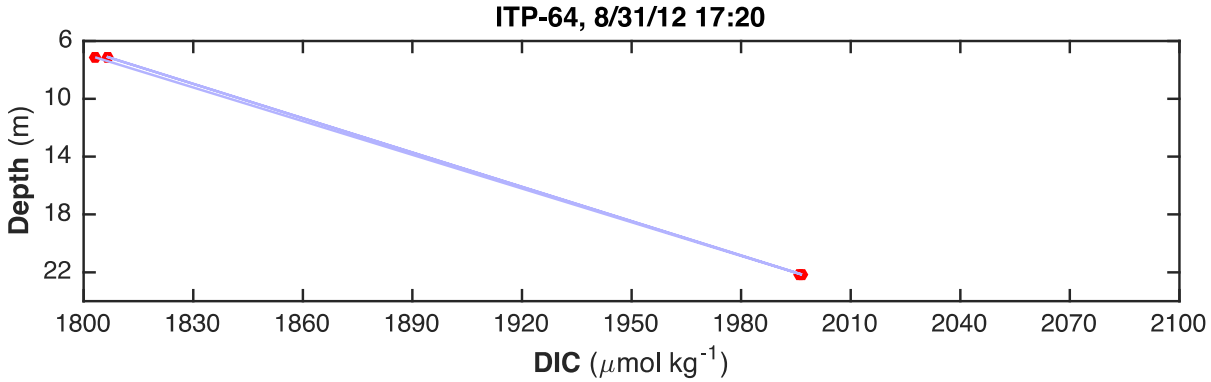

Figure 4.9. DIC (red dot) in the ITP-64 mixed layer. The date and time for the first sampling are included on top of the figure. Samplings were done at ~15 minute intervals. The average MLD at ITP-64 is 21.5 ± 2 m.

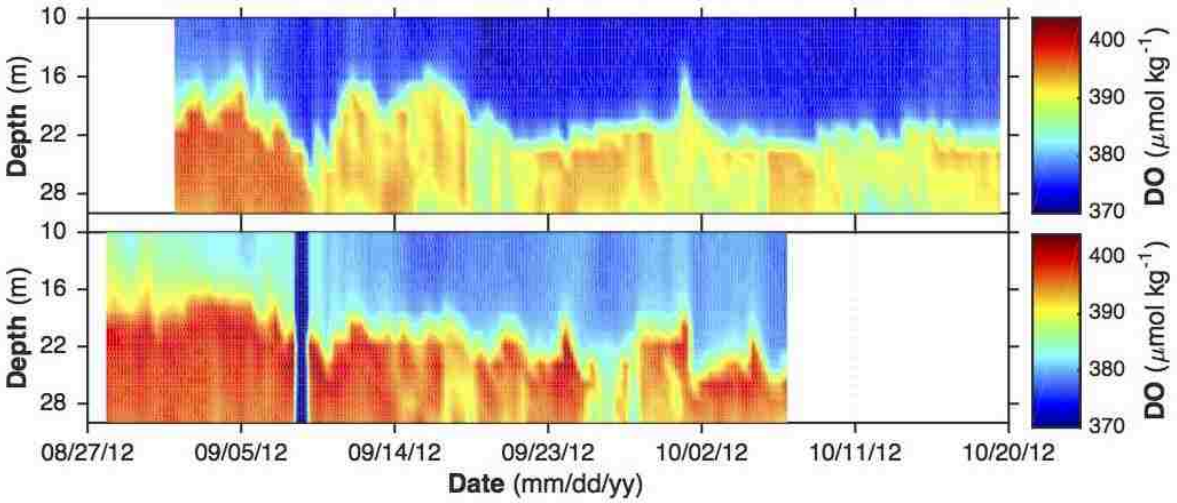

Figure 4.10. Depth-resolved time-series DO data. Top figure refers to ITP-64, bottom figure refers to ITP-65. The DO values are small in the mixed layer and larger at depths. The short-term variability in DO in the mixed layers presumably originated from the combination of large concentration gradients around the sensors and water movement driven by large-scale processes. At both ITPs, surface seawater was always supersaturated with respect to DO.

Since NCP in the Canada Basin is expected to be negligible except during summer due to significant ice-cover, we compared our estimates with other annual estimates in the region, though scarcity of data from the deep AO during late summer-autumn constrained our scope to make any direct comparison. When considered a 90-day open water period, the NCP is estimated to be 0.66 mol m^{-2} yr^{-1} at ITP-64 and ~0 mol m^{-2} yr^{-1} at ITP-65 and the GPP is 1.2 mol m^{-2} yr^{-1} and ~0 mol m^{-2} yr^{-1}, respectively. Subba Rao and Platt (1984) and Legendre *et al.* (1992) estimated phytoplankton production in offshore (depth > 200 m) central Arctic waters north of 65°N to be 0.75 mol m^{-2} yr^{-1}. Gosselin *et al.* (1997) reported an annual primary production of about 1.25 mol m^{-2} yr^{-1} in the central basin. Moran *et al.* (1997) found that the distribution of total primary production within the interior Arctic increases with latitude from ~ 1 mmol m^{-2} d^{-1} at ~ 82°N to ~ 5-28 mmol m^{-2} d^{-1} from 84-90°N. Bates *et al.* (2005) estimated the rate of NCP in the AO basin stations to be 0.18-0.54 mol m^{-2} yr^{-1}, when a growing season of 120 day was assumed. Anderson *et al.* (2003) reported annual primary production in the

AO to be on an average less than 0.04 mol m^{-2} yr^{-1}. All these estimates with our more recent estimates indicate that production in the Canada Basin is considerably low compared to shelf regions and other low-latitude oceans. Our estimates using ITP-64 and ITP-65 data also show that NCP in partially ice-covered water is significantly higher than that under multiyear sea ice, which corroborates earlier observations that leads of open water can enhance productivity (Gosselin *et al.* 1997; Sakshaug, 2004).

4.4. Gas Flux and NCP Comparison

The CO_2 gas flux rate and NCP at ITP-64 are very similar, 7.8 mmol m^{-2} d^{-1} and 7.4 mmol m^{-2} d^{-1}, suggesting that NCP counterbalanced gas exchange over the period of the study. This is probably why ITP-64 pCO_2 virtually stopped increasing half way through the measurement period. After 09/26/12, when no PAR is available and nutrients are likely depleted (Fig 4.2) and the ice coverage is still not heavy (~20%) (Fig. 3.1e), this counterbalanced coupling between CO_2 gas flux and NCP would, in theory, gradually wane as the upward trend in CO_2 would resume and DO would head towards saturation due to absence of biological activity. The increasing ice coverage toward the end of the measurement period is expected to continue which would gradually stop all significant gas exchange and NCP, at which point ITP-64 CO_2 and DO would be similar to ITP-65 pCO_2 and DO.

Chapter 5

Summary

Biogeochemical data collected from two ITPs provided insights into the inorganic carbon cycle and oxygen variability in the region. Our pCO_2 data show similar levels of pCO_2 in the Canada Basin compared to many previous data. In the case of both ITPs, pCO_2 and DO were undersaturated and slightly supersaturated, respectively, suggesting that DO in the shallow Arctic mixed layer equilibrates with the atmosphere relatively rapidly. ITP-64 data collected under sparse ice and ITP-65 data collected under multiyear ice were evaluated separately and comparatively with the help of biogeochemical models to assess the variability of pCO_2 and DO in seawater. ITP-64 pCO_2 and DO variability for the most part was linked to gas exchange and biological activity, though some of the variability was linked to salinity which was related to horizontal advection. Temperature had little overall effect, as there was not much warming and brine rejection did not appear to be important even under little ice cover where ice formation would presumably be significant as water reached freezing point. Horizontal gradients dominated pCO_2 variability in the densely ice-covered region with small gas exchange and negligible NCP in the surface. One interesting feature this study has revealed is that pCO_2 variability under heavy ice and little ice can be strikingly similar even when the contributions from gas exchange and photosynthesis are very different. Our CO_2 gas flux and NCP estimates in comparison with the wide range of previous estimates show that gas flux and NCP estimates are highly variable in space and time over the AO. Previous studies reported increases in primary production in the AO resulting from decreased sea ice extent and a longer phytoplankton growing season, though envisioned that future increases in production will slow down as surface nutrient inventories become depleted (Pabi et al., 2008,

Arrigo et al., 2008). Our estimates compared to previous reports found medium production in the partially ice-covered AO with nutrients in the mixed layer that is typically found in the subsurface Arctic waters (Arrigo et al., 2008), potentially as a result of wind-driven shelf-break upwelling (Carmack and Chapman, 2003).

It is likely that the pCO_2 levels in the surface water of the Canada Basin will move toward atmospheric saturation if the ice-free period continues to increase. We calculated Ω_{arag} at present pCO_2 levels and at atmospheric saturation (assuming atmospheric pCO_2 at 400 μatm) using CO2SYS. Under current conditions, Ω_{arag} at ITP-64 ranges from 1.03 to 1.16 with a mean of 1.08 ± 0.03. Under equilibrium conditions, ITP-64 Ω_{arag} ranges from 0.84 to 0.88 with a mean of 0.86 ± 0.01. Clearly, with sustained open water condition, equilibrium of surface seawater with the atmosphere would bring Ω_{arag} below 1 (Fig. 5.0), favoring aragonite dissolution. Undersaturation of the surface waters of the Canada Basin with respect to aragonite has already been observed (Yamamoto-Kawai *et al.*, 2009b). Since the preindustrial period, the increase in atmospheric CO_2, surface water warming, and melting of sea ice has lowered surface calcium carbonate saturation state in the Canada Basin by ~0.3, 0.1 and 0.4 units, respectively (Yamamoto-Kawai *et al.*, 2011). Under such conditions, the calcium carbonate shells of many marine organisms that support the fundamental food web in the ocean dissolve in seawater, jeopardizing the entire food chain in the ocean as well as on land.

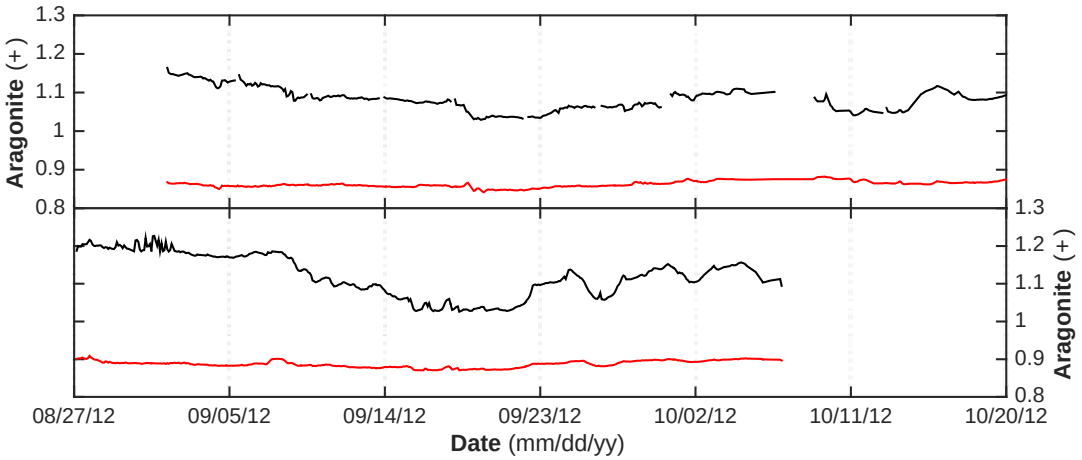

Figure 5.0 Aragonite saturation state (Ω_{arag}) at ITP-64 is shown on the top figure (black) and at ITP-65 on the bottom figure (black). Red lines refer to Ω_{arag} when assumed that seawater is in equilibrium with the atmosphere with respect to pCO_2. Equilibrium between seawater and atmosphere brings Ω_{arag} below 1, favoring aragonite dissolution.

To our knowledge, no under ice and partially open water Arctic pCO_2 and O_2 data have been compared before, though an appropriate comparison between under ice and open water or nearly open water biogeochemical data sets from the AO is challenging due to heterogeneous distribution of sea ice cover. The dynamic nature of sea ice (e.g. drifting, melting, melt ponds) further contributes to this heterogeneity, making the biogeochemical environment even more complex. Therefore, more open water and under ice studies are needed to gain confidence in our understanding of processes and controls that regulate pCO_2 and O_2 variability in the AO.

Chapter 6

Conclusions

The major findings and implications of this study are:

(1) Gas exchange, NCP and horizontal gradients are the main sources of the CO_2 and O_2 variability in the partially ice-covered Arctic Ocean.

(2) pCO_2 and O_2 differed significantly in contributions from gas exchange and NCP under sparse ice and multiyear ice cover.

(3) The pCO_2 under heavy ice and little ice were strikingly similar even though contributions from gas exchange and photosynthesis were quite different.

(4) Horizontal gradients dominated the more densely ice-covered regions, with no significant NCP in the surface.

(5) Equilibrium of Arctic seawater CO_2 with the atmosphere would bring aragonite saturation state below 1.

References:

Aagaard, K., and E. Carmack (1989), The role of sea ice and other fresh water in the Arctic circulation, J. Geophys. Res., 94, 14,485–14,498.

Anderson, L. G., Dyrssen, D., and Jones, E. P. (1990), An assessment of the transport of atmospheric CO_2 into the Arctic Ocean, J. Geophys. Res., 95(C2), 1703–1711.

Anderson, L. G., Olsson, K., and Skoog, A. (1994), Distribution of dissolved inorganic and organic carbon in the Eurasian Basin of the Arctic Ocean, in The Polar Oceans and Their Role in Shaping the Global Environment, edited by Johannessen, O. M., Muench, R. D., and Overland, J. E., American Geophysical Union, Geophysical Monograph, 85, 252–262.

Anderson, L. G., Olsson, K., Jones, E. P., Chierici, M., and Fransson, A. (1998), Anthropogenic carbon dioxide in the Arctic Ocean: Inventory and sinks, J. Geophys. Res., 10(C12), 27707–27716.

Aagaard, K. and Woodgate, R. A. (2001), Some thoughts on the freezing and melting of sea ice and their effcts on the ocean. Ocean Modelling, Volume 3, Issues 1–2, 2001, Pages 127–135. doi:10.1016/S1463-5003(01)00005-1.

Altabet M.A., Ryabenko E, Stramma L., Wallace DWR, Frank M. (2012), An eddy-stimulated hotspot for fixed nitrogen-loss from the Peru oxygen minimum zone. Biogeoscience 9: 4897–4908.

Anderson, L. G., Jutterstrom, S., Hjalmarsson, S. H., Wahlstrom, I., and Semiletov, I. P. (2009), Out-gassing of CO_2 from Siberian Shelf seas by terrestrial organic matter decomposition, Geophys. Res. Lett., 36, L20601, doi: 10.1029/2009GL040046.

Anderson, L. G., E. P. Jones, and J. H. Swift (2003), Export production in the central Arctic Ocean evaluated from phosphate deficits, J. Geophys. Res., 108(C6), 3199, doi:10.1029/2001JC001057.

Anderson, L. G., and S. Kaltin (2001), Carbon fluxes in the Arctic Ocean- Potential impact by climate change, Polar Res., 20(2), 225– 232.

Anderson, L. G., K. Olsson, and M. Chierici. (1998), A carbon budget for the Arctic Ocean. Global Biogeochemical Cycles 12:455–465.

Apollonio, S. (1959), Hydrobiological measurements on IGY Drifting Station Bravo. Transactions, American Geophysical Union, 40,316-3 19.

Arrigo, K. R., et al. (2012), Massive phytoplankton blooms under Arctic sea ice, Science, 336 (6087), 1408-1408, doi: 10.1126/science.1215065.

Arrigo, K. R., G. van Dijken, and S. Pabi (2008), Impact of a shrinking Arctic ice cover on marine primary production, Geophys. Res. Lett., 35, L19603, doi:10.1029/2008GL035028.

Bates, N. R. and Mathis, J. T (2009), The Arctic Ocean marine carbon cycle: evaluation of air-sea exchanges, ocean acidification impacts and potential feedbacks, Biogeosciences, 6, 2433-2459, doi:10.5194/bg-6-2433-2009.

Bates, N. R (2007), Interannual variability of the oceanic CO_2 sink in the subtropical gyre of the North Atlantic Ocean over the last two decades, J. Geophys. Res. Oceans, 112, C09013, doi: 2006JC003759.

Bates, N. R. (2006), Air-sea CO_2 fluxes and the continental shelf pump of carbon in the Chukchi Sea adjacent to the Arctic Ocean, J. Geo- phys. Res. Oceans, 111, C10013, doi:10.129/2005JC003083.

Bates, N. R., Margaret H.P. B., Hansell, D.A. (2005), Spatio-temporal distribution of dissolved inorganic carbon and net community production in the Chukchi and Beaufort Seas, Deep-Sea Research II, 52 (2005) 3303–3323, doi:10.1016/j.dsr2.2005. 10.005.

Boetius, A. *et al.* (2013), Export of algal biomass from the melting Arctic sea ice. Science, 339,1430-1432.

Bopp, L., C. Le Que´re´, M. Heimann, A. C. Manning, and P. Monfray (2002), Climate-induced oceanic oxygen fluxes: Implications for the contemporary carbon budget, Global Biogeochem. Cycles, 16(2), 1022, doi:10.1029/2001GB001445.

Borges, A. V. (2005), Do we have enough pieces of the jigsaw to integrate CO_2 fluxes in the coastal ocean? Estuaries, 28(1), 3–27.

Borges, A. V. (2011), Oceans and the Atmospheric Carbon Content, Springer, Ch. Present Day Carbon Dioxide Fluxes in the Coastal Ocean and Possible Feedbacks Under Global Change, pp. 47–63.

Borges, A. V., Delille, B., and Frankignoulle, M. (2005), Budgeting sinks and sources of CO_2 in the coastal ocean: Diversity of ecosystems counts, Geophys. Res. Lett., 32, L14601, doi:10.1029/2005GL023053.

Cai W-J., *et al.* (2010), Decrease in the CO2 Uptake Capacity in an Ice-Free AO Basin, Science 329, 556 (2010), doi: 10.1126/science.1189338.

Cai, W.-J. and Dai, M. (2004), A Comment on "Enhanced open ocean storage of CO_2 from shelf sea pumping", Science, 306, 1477c.

Cai, W.-J., Dai, M., and Wang, Y. (2006), Air-sea exchange of carbon diox- ide in ocean margins: A province-based synthesis, Geophys. Res. Lett., 33, L12603, doi: 10.1029/2006GL026219.

Carmack, E. C., and D. Chapman (2003), Wind-driven shelf/basin exchange on an Arctic shelf: The joint roles of ice cover extent and shelf-break bathymetry, Geophys. Res. Lett., 30(14), 1778, doi: 10.1029/2003GL017526.

Carmack, E. and Wassmann, P. (2006), Food webs and physical- biological coupling on pan-Arctic shelves: Unifying concepts and comprehensive perspectives, Prog. Oceanogr., 71, 446–477, doi:10.1016/j.pocean.2006.10.004.

Chang BX, Devol AH (2009), Seasonal and spatial patterns of sedimentary denitrification rates in the Chukchi Sea, Deep-Sea Res Part II, 56(17): 1339–1350.

Chapin, F. S., III, *et al.* (2005a), Polar systems. Pages 717–743 in H. Hassan, R. Scholes, and N. Ash, editors, The millenium ecosystem assessment. Island Press, Washington, D.C., USA.

Chapin, F. S., III, *et al.* (2005b), Role of land-surface changes in arctic summer warming, Science 310:657–660.

Chen, C.-T. A., Liu, K.-K., and Macdonald, R. W. (2003), Continental margin exchanges. Pages 53–97 in M. J. R. Fasham, editor. Ocean biogeochemistry: the role of the ocean carbon cycle in global change, Springer-Verlag, Berlin, Germany.

Chen, M., Huang, Y.P., Guo, L.D., Cai, P.H., Yang, W.F., Liu, G.S., Qiu, Y.S. (2002), Biological productivity and carbon cycling in the Arctic Ocean Chinese Science Bulletin, 47 (12) (2002), pp. 1037–1040.

Chen, C. T. A. and Borges, A. V. (2009), Reconciling opposing views on carbon cycling in the coastal ocean: Continen- tal shelves as sinks and near-shore ecosystems as sources of atmospheric CO_2. Deep-Sea Res. II, 56(8–10), 578–581, doi:10.1016/j.dsr2.2009.01.001.

Codispoti, L. A., V. Kelly, A. Thessen, P. Matrai, S. Suttles, V. Hill, M. Steele, and B. Light (2013), Synthesis of primary production in the Arctic Ocean: III. Nitrate and phosphate based estimates of net community production. Progress in Oceanography, 110, 126-150, doi:10.1016/j.pocean.2012.11.006.

Cota, G. F., Pomeroy, L. R., Harrison, W. G., Jones, E. P., Peters, F. Sheldon, Weingartner, W. M. (1996), Nutrients, primary production and microbial heterotrophy in the south-eastern Chukchi Sea: Arctic summer nutrient depletion and heterotrophy, Marine Ecology Progress Series, 135 (1–3) (1996), pp. 247–258.

Cross, J. N., J. T. Mathis, N. R. Bates, and R. H. Byrne (2013), Conservative and non-conservative variations of total alkalinity on the south-eastern Bering Sea shelf, Mar. Chem., 154, 100–112, doi:10.1016/j.marchem.2013.05.012.

Cullen, J. J., M. R. Lewis, C. O. Davis, and R. T. Barber (1992), Photosynthetic characteristics and estimated growth rates indicate grazing is the proximate control of primary production in the equatorial Pacific, J. Geophys. Res., 97, 630–654.

DeGrandpre, M.D., Körtzinger, A., Send, U., Wallace, D.W.R. and R.G.J. Bellerby (2006), Uptake and sequestration of atmospheric CO2 in the Labrador Sea deep convection region, Geophys. Res. Lett. 33, doi:10.1029/2006GL026881.

DeGrandpre, M.D., Wanninkhof, R., McGillis, W.R. and P. Strutton (2004), A Lagrangian study of pCO2 dynamics in the eastern equatorial Pacific Ocean, J. Geophys. Res. - Oceans, 109, doi10.1029/2003JC002089.

DeGrandpre, M.D., Olbu, G.J., Beatty, C.M. and T.R. Hammar (2002), Air-sea CO2 fluxes on the U.S. Middle Atlantic Bight, Deep-Sea Res. II, 49, 4355-4367.

DeGrandpre, M.D., Baehr, M.M. and T.R. Hammar (1999), Calibration free optical chemical sensors, Anal. Chem., 71, 1152-1159.

DeGrandpre, M.D., Hammar, T.R. and C.D. Wirick. (1998), Short term pCO_2 and O_2 dynamics in California coastal waters, Deep-Sea Res. Part II, 45, 1557-1575.

DeGrandpre, M.D., Hammar, T.R., Wallace, D.W.R., and C.D. Wirick (1997), Simultaneous mooring-based measurements of seawater CO_2 and O_2 off Cape Hatter-as, North Carolina, Limnol. Oceanog., 42, 21-28.

DeGrandpre, M.D., Hammar, T.R., Smith, S.P., and F.L. Sayles. (1995). *In situ* measurements of seawater pCO_2. Limnol. Oceanog., 40, 969-975.

Dickson, A. G., Sabine, C. L., Christian, J. R. (2007), Guide to Best Practices for Ocean CO_2 Measurements, North Pacific Marine Science Organization, Sydney, British Columbia.

Dugdale and Goering (1967). Uptake of new and regenerated forms of nitrogen in primary productivity. Limnology and Oceanography. Volume 12, Issue 2, pages 196–206. doi: 10.4319/lo.1967.12.2.0196

Else G. T., Galley R. J., Lansard B., Barber D. G., Brown K., Miller L. A., Mucci A., Papakyriakou T. N., Tremblay J.-É., and Rysgaard S. (2013), Further observations of a decreasing atmospheric CO_2 uptake capacity in the Canada Basin (Arctic Ocean) due to sea ice loss. Geophysical Research Letters, VOL. 40, 1132-1137, doi:10.1002/grl.50268.

Else, B. G. T., T. N. Papakyriakou, R. J. Galley, A. Mucci, M. Gosselin, L. A. Miller, E. H. Shadwick, and H. Thomas (2012a), Annual cycles of pCO2sw in the southeastern Beaufort Sea: New understandings of air-sea CO_2 exchange in Arctic polynya regions, J. Geophys. Res., 117, C00G13, doi:10.1029/2011JC007346.

Else, B. G. T., R. J. Galley, T. N. Papakyriakou, L. A. Miller, A. Mucci, and D. Barber (2012b), Sea surface pCO_2 cycles and CO_2 fluxes at landfast sea ice edges in Amundsen Gulf, Canada, J. Geophys. Res., 117, C09010, doi: 10.1029/2012JC007901.

Emerson, S., Sabine, C.L., Cronin, M., Cullison, S.E., and M.D. DeGrandpre (2011), Production rates of $CaCO_3$ and organic carbon in ocean surface waters from *in situ* measurements of pCO_2 and pH, Global Biogeochem. Cycles, 25, GB3008, doi:10.1029/2010GB003.

Fanning, K. A., and L. M. Torres (1991), Rn-222 and Ra-226—Indicators of sea-ice effects on air-sea gas-exchange, Polar Res., 10(1), 51–58.

Fransson, A., Chierici, M., and Nojiri, Y. (2009). New insights into the spatial variability of the surface water carbon dioxide in varying sea ice conditions in the Arctic Ocean, Cont. Shelf Res., 29(10), 1317–1328, doi:10.1016/j.csr.2009. 03.008.

Giles, K. A., S. W. Laxon, and A. L. Ridout (2008), Circumpolar thinning of Arctic sea ice following the 2007 record ice extent minimum, Geophys. Res. Lett., 35(22), doi:10.1029/2008GL035710.

Gnaiger, E., Forstner, H. (1983), Polarographic Oxygen Sensors: Aquatic and Physiological Applications, Page 326.

Gosselin, M., Levasseur, M., Wheeler, P.A., Horner, R.A., Booth, B.C. (1997), New measurements of phytoplankton and ice algal production in the Arctic Ocean. Deep-Sea Research II, 44 (1997), pp. 1623–1644.

Hamme, R. C., and S. R. Emerson (2004), The solubility of neon, nitrogen and argon in distilled water and seawater, Deep Sea Res., Part I, 51(11), 1517–1528.

Hill, V. J., and G. F. Cota (2005), Spatial patterns of primary production in the Chukchi Sea in the spring and summer of 2002, Deep Sea Res., Part II, 52, 3344–3354.

Hinzman, L. D., et al. (2005), Evidence and implications of recent climate change in terrestrial regions of the Arctic, Climatic Change 72:251–298.

Hood, E. M., B. L. Howes, and W. J. Jenkins (1998), Dissolved gas dynamics in perennially ice-covered Lake Fryxell, Antarctica, Limnol. Oceanogr., 43(2), 265–272.

Honjo, S., Krishfield, R.A., Eglinton, T.I., Manganini, S.J., Kemp, J.N., Doherty, K., Hwang, J., McKee, T.K., and Takizawa, T. June (2010), Biological pump processes in the cryopelagic and hemipelagic Arctic Ocean: Canada Basin and Chukchi Rise. Progress In Oceanography, Volume 85, Issues 3-4, pages 137-170.

Jackson, J.M., W.J. Williams and E.C. Carmack (2012), Winter sea-ice melt in the Canada Basin, Arctic Ocean. Geophys. Res. Lett., 39, L03603, doi:10.1029/2011GL050219.

Jakobsson, M., *et al.* (2012), The International Bathymetric Chart of the Arctic Ocean (IBCAO) Version 3.0, Geophysical Research Letters, doi: 10.1029/2012GL052219.

Jakobsson, M. (2002), Hypsometry and volume of the AO and its constituent's seas, Geochemistry Geophysics Geosystems, v. 3, no. 2.

Johnson, G. C., and N. Gruber (2007), Decadal water mass variations along 20°W in the northeastern Atlantic Ocean. Prog. Oceanogr., 73, 277–295. doi:10.1016/j.pocean.2006.03.022.

Jutterström, S. and L. G. Anderson (2010), Uptake of CO_2 by the Arctic Ocean in a changing climate, Mar. Chem., 122, 96–104. doi:10.1016/j. marchem. 2010.07.002.

Kaltin, S., and L. G. Anderson (2005), Uptake of atmospheric carbon dioxide in Arctic shelf seas: Evaluation of the relative importance of processes that influence pCO_2 in water transported over the Bering- Chukchi Sea shelf, Mar. Chem., 94, 67-79.

Kalvelage T, Lavik G, Lam P, Contreras S, Arteaga L, (2013), Nitrogen cycling driven by organic matter export in the South Pacific oxygen minimum zone, Nature Geosci 6: 228–234.

Kay, J. E., T. L'Ecuyer, A. Gettelman, G. Stephens, and C. O'Dell (2008), The contribution of cloud and radiation anomalies to the 2007 arctic sea ice extent minimum, Geophys. Res. Lett., 35, L08503, doi:10.1029/2008GL033451.

Killawee, J. A., I. J. Fairchild, J.-L. Tison, L. Janssens, and R. Lorrain (1998), Segregation of solutes and gases in experimental freezing of dilute solutions: Implications for natural glacial systems, Geochim. Cosmochim. Acta, 62, 3637–3655.

Koerner, R. M. (1970), Some observations on superimposition of ice on the Devon Island Ice Cap, N.W.T., Canada. Geogr. Ann., Vol.52A, pp.57-67.

Krishfield, R., J. Toole, A. Proshutinsky, and M.-L. Timmermans (2008a), Automated Ice-Tethered Profilers for seawater observations under pack ice in all seasons. Journal of Atmospheric and Oceanic Technology, Vol. 25, doi: 10.1175/ 2008JTECHO587.1.

Krishfield, R., J. Toole, and M.-L. Timmermans (2008b), ITP Data Processing Procedures, Woods Hole Oceanographic Institution, 24 pp. Available online at: http://www.whoi.edu/page.do?pid=23096 (accessed August 24, 2015).

Kuss, J., Roeder, W., Wlost, K., and M. DeGrandpre (2006), Time-series of surface water CO_2 and oxygen measurements on a plat-form in the central Arkona Sea (Baltic Sea): Seasonality of uptake and release, Mar. Chem., 101, 220-232.

Lansard, B., A. Mucci, L. A. Miller, R. W. Macdonald, and Y. Gratton (2012), Seasonal variability of water mass distribution in the southeastern Beaufort Sea determined by total alkalinity and d18O, J. Geophys. Res., 117, C03033, doi:10.1029/2011JC007299.

Legendre, L., Ackley, S. F., Dieckmann, G. S., Gulliksen, B., Homer, R., Hoshiai, T., Melnikov, I. A., Reeburgh, W. S., Spindler, M. and Sullivan, C. W. (1992), Ecology of sea ice biota 2, Global significance, Polar Biology, 12,429-444.

Lewis, E., and D. W. R. Wallace, (1998), ORNL/CDIAC-105, Carbon Dioxide Information Analysis Center, Oak Ridge National Laboratory, U.S. Department of Energy, Oak Ridge, Tennessee.

Lewis, E.L. and Perkins, R.G. (1983). Supercooling and energy exchange near the Arctic Ocean surface. Journal of Geophysical Research 88: doi: 10.1029/JC088iC12p07681. issn: 0148-0227.

Lundberg, L., and P. M. Haugan (1996), A Nordic Seas–Arctic Ocean carbon budget from volume flows and inorganic carbon data, Global Biogeochemical Cycles 10:493–510.

Loose, B., W. R. McGillis, P. Schlosser, D. Perovich, and T. Takahashi (2009), Effects of freezing, growth, and ice cover on gas transport processes in laboratory seawater experiments, Geophys. Res. Lett., 36, L05603, doi:10.1029/2008GL036318.

Loose, B., W. R. McGillis, D. Perovich, C. J. Zappa, and P. Schlosser (2014), A parameter model of gas exchange for the seasonal sea ice zone, Ocean Sci., 10(1), 17–28.

Macdonald, R. W. Anderson, L. G., Christensen, J. P., Miller, L. A., Semiletov, I. P., and Stein, R. (2009), The Arctic Ocean, in: Carbon and Nutrient Fluxes in Continental Mar-

gins: A Global Syn-thesis, edited by: Liu, K. K., Atkinson, L., Quinones, R., and Talue-McManus, L., Global Change - The IGBP Series, Springer, New York, USA, 291–303.

Manizza, M., M. J. Follows, S. Dutkiewicz, D. Menemenlis, C. N. Hill, and R. M. Key (2013), Changes in the Arctic Ocean CO_2 sink (1996–2007): A regional model analysis, Global Biogeochem. Cycles, 27, doi: 10.1002/2012GB004491.

Martz, T.M., DeGrandpre, M.D., Strutton, P.G., McGillis, W.R. and W. Drennan. (2009), Sea surface pCO_2 and carbon export during the Labrador Sea spring-summer bloom: an in situ mass balance approach, J. Geophys. Res.-Oceans, 114, C09008, doi: 10.1029/2008JC005.

Maslanik, J. A., Fowler, C., Stroeve, J., Drobot, S., Zwally, J., Yi, D. and W. Emery (2007), A younger, thinner Arctic ice cover: Increased potential for rapid, extensive sea-ice loss, Geophys. Res. Lett., 34, L24501, doi:10.1029/2007GL0320 43.

Mathis, J. T., et al. (2012), Storm-induced upwelling of high pCO_2 waters onto the continental shelf of the western Arctic Ocean and implications for carbonate mineral saturation states, Geophys. Res. Lett., 39, L07606, doi:10.1029/2012GL051574.

Matear, R. J. (2000), Climate change impacts on marine systems, Aust. Microbiol., 21(2), 17-20.

McPhee, M. G., A. Proshutinsky, J. H. Morison, M. Steele, and M. B. Alkire (2009), Rapid change in freshwater content of the Arctic Ocean, Geophys. Res. Lett., 36, L106 02, doi:10.1029/2009 GL037525.

McGuire, A. D., Anderson, L. G., Christensen, T. R., Dallimore, S., Guo, L., Hayes, D. J., Heimann, M., Lorenson, T. D., Macdonald, R. W., and Roulet, N. (2009), Sensitivity of the carbon cycle in the Arctic to climate change, Ecol. Monogr., 79, 523–555.

McGuire, A. D., and F. S. Chapin, III. (2006). Climate feedbacks in the Alaskan boreal forest. Pages 309–322 in F. S. Chapin, III, M. W. Oswood, K. Van Cleve, L. A. Viereck, and D. L. Verbyla, editors, Alaska's changing boreal forest. Oxford University Press, New York, New York, USA.

McGuire, A. D., F. S. Chapin, III, J. E. Walsh, and C. Wirth. (2006), Integrated regional changes in arctic climate feedbacks: implications for the global climate system. Annual Review Environment and Resources 31:61–91.

McLaughlin, F., E. Carmack, A. Proshutinsky, R.A. Krishfield, C. Guay, M. Yamamoto-Kawai, J.M. Jackson, and B. Williams (2011), The rapid response of the Canada Basin to climate forcing: From bellwether to alarm bells, Oceanography 24(3):146–159,

http://dx.doi.org/10.5670/oceanog.2011.66.

Mecking, S., C. Langdon, R. A. Feely, C. L. Sabine, C. A. Deutsch, and D-H. Min (2008), Climate variability in the North Pacific thermocline diagnosed from oxygen measurements: An update based on the U.S. CLIVAR/CO_2 Repeat Hydrography cruises, Global Biogeochem, Cycles, 22, GB3015. doi:10.1029/2007GB003101.

Mellor, G. L., M. G. McPhee, and M. Steele (1986), Ice-seawater turbulent boundary layer interaction with melting or freezing, J. Phys. Oceanogr., 16, 1829–1846.

Millero F. J., Leung W. H. (1976), The thermodynamics of seawater at one atmosphere. American Journal of Science. 276:1035-1077.

Moore, T. S., DeGrandpre, M. D., Sabine, C. L., Zappa, C. J., McGillis, W. R., Feely, R. A., Hamme, R. C. and W. M. Drennan (2011), Sea surface pCO_2 and O_2 in the Southern Ocean during the austral fall, 2008, J. Geophys. Res.-Oceans, 116, C00F11, doi:10.1029/2010JC006560.

Moran, S. B., Ellis, K. M., Smith, J. N. (1997), $^{234}Th/^{238}U$ disequilibrium in the central Arctic Ocean: implications for particulate organic carbon export, Deep-Sea Research II, 44 (1997), pp. 1593–1606.

Morison, J., R. Kowk, C. Peralta-Ferriz, M. Alkire, I. Rigor, R. Anderson and M. Steele (2012), Changing Arctic Ocean freshwater pathways, Nature, 481, doi:10.1038/ nature10705.

Mucci, A., B. Lansard, L. A. Miller, and T. N. Papakyriakou (2010), CO_2 fluxes across the air-sea interface in the southeastern Beaufort Sea: Icefree period, J. Geophys. Res., 115, C04003, doi:10.1029/2009JC005330.

Murata, A., and T. Takizawa (2003), Summertime CO_2 sinks in shelf and slope waters of the western Arctic Ocean, Cont. Shelf Res., 23(8), 753-776.

Nicolaus, M., C. Katlein, J. Maslanik, and S. Hendricks (2012), Changes in Arctic sea ice result in increasing light transmittance and absorption, Geophys. Res. Lett., 39, L24501, doi:10.1029/2012GL053738.

Nomura, D., H. Yoshikawa-Inoue, and T. Toyota (2006), The effect of sea-ice growth on air-sea CO2 flux in a tank experiment, Tellus, Ser. B, 58, 418–426.

Olli K., Wassmann P., Reigstad M., Ratkova T. N., Arashkevich E., Pasternak A., Matrai P. A., Knulst J., Tranvik L., Klais R., Jacobsen A. (2007), The fate of production in the central Arctic Ocean - top-down regulation by zooplankton expatriates? Prog. Oceanogr.

72, 84–113.

Overland, J. E., Wang, M., and Salo, S. (2008), The recent Arctic warm period, Tellus A, 60(4), 589–597, doi:10.1111/j.1600-0870.2008.00327.x.

Pabi, S., van Dijken, G. L., and Arrigo, K. R. (2008), Primary production in the Arctic Ocean, 1998–2006, J. Geophys.Res.. 113(C8), C08005, doi:10.1029/2007JC0045 78.

Parkinson C. L., Comiso J. C. (2013), On the 2012 record low Arctic sea ice cover: combined impact of preconditioning and an August storm. Geophys Res Lett 40:1356–1361.

Parmentier, F. J. W., Christensen, T. R., Sørensen, L. L., Rysgaard, S., McGuire, A. D., Miller, P. A., Walker, D. A. (2013), The Impact of Lower Sea Ice Extent on Arctic Greenhouse-Gas Exchange. Nature Climate Change, 3, 195-202, doi:10.1038/nclimate1784.

Penta, B., Z. Lee, R. Kudela, S. Palacios, D. Gray, J. Jolliff, and I. Shulman (2008), An Underwater Light Attenuation Scheme for Marine Ecosystem Models, Optics Express 16, pp. 16581-16591.

Perovich, K., Grenfell, T. C., Richter-Menge, J. A., Light, B., Tucker, W. B. and H. Eicken (2003), Thin and thinner: Sea ice mass balance measurements during SHEBA, J. Geophys. Res., 108, 8050, doi:10.1029/2001JC001079.

Perovich, D. K., Light, B., Eicken, H., Jones, K. F., Runciman, K. and S. V. Nghiem (2007), Increasing solar heating of the AO and adjacent seas, 1979-2005: Attribution and role in the ice-albedo feedback. Geophys. Res. Lett., 34, L19505, doi: 10.1029/2007GL031480.

Polyakov, I. V., Alekseev, G. V., Timokhov, L. A., Bhatt, U. S., Colony, R. L., Simmons, H. L., Walsh, D., Walsh, J. E., and Zakharov, V. F. (2002a), Variability of the intermediate Atlantic water of the Arctic Ocean over the last 100 years, J. Clim., 17(23), 4485-4497, doi:10.1175/JCLI-3224.1.

Polyakov, I. D., G. V. Alekseev, R. V. Bekryaev, U. Bhatt, R. Colony, M. A. Johnson, V. P. Karklin, A. P. Makshtas, D. Walsh, and A. V. Yulin (2002b), Observationally based assessment of polar amplification of global warming, Geophysical Research Letters 29:1878.

Platt, T., Gallegos, C. L., Harrison, W. G. (1980), Photo-inhibition of photosynthesis in natural assemblages of marine phytoplankton. J. Mar. Res. 38: 687–701.

Plattner, G. K., F. Joos, T. F. Stocker, and O. Marchal (2001), Feedback mechanisms and sensitivities of ocean carbon uptake under global warming, Tellus Ser. B, 53(5), 564– 592.

Poisson, A., and C. T. A. Chen (1987), Why is there little anthropogenic CO2 in the Antarctic bottom water, Deep Sea Res., Part A, 34(7), 1255–1275.

Polovina, J. J., E. A. Howell, and M. Abecassis (2008), Ocean's least productive waters are expanding, Geophys. Res. Lett., 35(3), L03618. http://dx.doi.org/10.1029/2007GL031745.

Popova, E. E., A. Yool, A. C. Coward, Y. K. Aksenov, S. G. Alderson, B. A. de Cuevas, and T. R. Anderson (2010), Control of primary production in the Arctic by nutrients and light: Insights from a high resolution ocean general circulation model, Biogeosciences, 7(11), 3569–3591, doi:10.5194/bg-7-3569-2010.

Popova, E. E., Yool, A., Coward, A. C., Dupont, F., Deal, C., Elliott, S., Hunke, E., Jin, M., Steele, M., Zhang, J. (2012), What controls primary production in the Arctic Ocean? Results from an intercomparison offive general circulation models with biogeochemistry. J. Geophys. Res. 117, C00D12. http://dx.doi.org/10.1029/2011 JC007112.

Proshutinsky, A., R. Krishfield, M.-L. Timmermans, J. Toole, E. Carmack, F. McLaughlin, W. J. Williams, S. Zimmermann, M. Itoh, and K. Shimada (2009), Beaufort Gyre freshwater reservoir: State and variability from observations, J. Geophys. Res., 114, C00A10, doi: 10.1029/2008JC005104.

Redfield A. C. (1934), On the proportions of organic derivations in sea water and their relation to the composition of plankton, In James Johnstone Memorial Volume. (ed. R.J. Daniel). University Press of Liverpool, pp. 177–192, 1934.

Robbins LL, et al. (2013), Baseline Monitoring of the Western Arctic Ocean Estimates 20% of Canadian Basin Surface Waters Are Undersaturated with Respect to Aragonite, PLoS ONE 8(9): e73796. doi: 10.1371/journal.pone.0073796.

Rutgers van der Loeff, M. M., N. Cassar, M. Nicolaus, B. Rabe, and I. Stimac (2014), The influence of sea-ice cover on air-sea gas exchange estimated with radon-222 profiles, J. Geophys. Res. Oceans, 119, 2735–2751, doi:10.1002/2013JC009321.

Rysgaard, S., R. N. Glud, M. K. Sejr, J. Bendtsen, and P. B. Christensen (2007), Inorganic carbon transport during sea ice growth and decay: A carbon pump in polar seas, J. Geophys. Res., 112, C03016, doi:10.1029/2006JC003572.

Sakshaug, E. (2004), Primary and secondary production in the Arctic Seas, in The Organic Carbon Cycle in the Arctic Ocean, edited by R. Stein and R. Macdonald, pp. 57–81, Springer, Berlin Heidelberg.

Santana-Casiano, J. M., Gonzalez-Davila, M., Rueda, M.-J., Lli- nas, O., and Gonzalez-

Davila, E.-F (2007), The interannual variability of oceanic CO_2 parameters in the western Atlantic subtropical gyre at the ESTOC site, Global Biogeochem. Cy., 21, GB1015, doi:10.1029/2006GB002788.

Sarmiento, J. L., T. M. C. Hughes, R. J. Stouffer, and S. Manabe (1998), Simulated response of the ocean carbon cycle to anthropogenic climate warming, Nature, 393, 245–249.

Semiletov, I. P. and Pipko, I. I. (2007), Sinks and sources of carbon dioxide in the Arctic Ocean: Results of direct instrumental measurements, Dokl. Earth Sci., 414, 642–645.

Serreze, M. C., A. P. Barrett, A. G. Slater, R. A. Woodgate, K. Aagaard, R. B. Lammers, M. Steele, R. Moritz, M. Meredith, and C. M. Lee. (2006), The large-scale freshwater cycle of the Arctic. Journal of Geophysical Research 111: C11010.

Serreze, M. C. and Francis, J. A. (2006), The Arctic amplification debate, Clim. Change, 76, 241-264.

Serreze, M. C., J. E. Walsh, F. S. Chapin, III, T. Osterkamp, M. Dyurgerov, V. Romanovsky, W. C. Oechel, J. Morison, T. Zhang, and R. G. Barry. (2000), Observational evidence of recent change in the northern high-latitude environment, Climatic Change 46:159–207.

Serreze, M. C. Holland, M. M. and J. Stroeve (2007), Perspectives on the Arctic's shrinking sea ice cover. Science, 315, 1533-1536.

Shadwick, E. H., et al. (2011), Seasonal variability of the inorganic carbon system in the Amundsen Gulf region of the southeastern Beaufort Sea, Limnol. Oceanogr., 56(1), 303–322, doi:10.4319/lo.2011.56.1.0303.

Slagstad, D., I. H. Ellingsen, and P. Wassmann (2011). Evaluating primary and secondary production in an Arctic Ocean void of summer sea ice: An experimental simulation approach, Prog. Oceanogr., 90, 117–131.

Smith, S. V. and Hollibaugh, J. T. (1995), Coastal metabolism and the oceanic organic carbon balance, Rev. Geophys., 31, 75–89.

Spitzer, W. S., and W. J. Jenkins (1989), Rates of vertical mixing, gas-exchange and new production - Estimates from seasonal gas cycles in the upper ocean near Bermuda, J. Mar. Res., 47(1), 169–196.

Spreen, G., R. Kwok, and D. Menemenlis (2011), Trends in Arctic sea ice drift and role of wind forcing: 1992–2009, Geophys. Res. Lett., 38, L19501, doi:10.1029/2011GL048970.

Stein, R., and R. W. Macdonald (2004), Arctic Ocean organic carbon accumulation and its global significance. Pages 315-322 in R. Stein and R. W. Macdonald, editors, The organic carbon cycle in the Arctic Ocean, Springer, Berlin, Germany.

Steinacher, M., Joos, F., Frölicher, T. L., Plattner, G.-K., and S.C. Doney (2009), Imminent ocean acidification in the Arctic projected with the NCAR global coupled carbon cycle-climate model, Biogeosciences, 6, 515-533.

Stramma, L., G. C. Johnson, J. Sprintall, and V. Mohrholz (2008), Expanding oxygen-minimum zones in the tropical oceans, Science, 320, 655–658.

Subba Rao, D. V. and Platt, T. (1984), Primary production of Arctic waters, Polar Biology, 3, 191-201.

Sundquist, E. T., (1985), Geological perspectives on carbon dioxide and the carbon cycle, in The Carbon Cycle and Atmospheric CO_2: Natural Variations Archean to Present, Geophys. Monogr. Ser., vol. 32, edited by E. T. Sundquist, and W. S. Broecker, pp. 5–59, AGU, Washington, D. C.

Takahashi, T., J. Olafsson, J. G. Goddard, D. W. Chipman, and S. C. Sutherland (1993), Seasonal variation of CO_2 and nutrients in the high-latitude surface oceans: A comparative study, Global Biogeochemical Cycles 7:843–878.

Takahashi, T., S. C. Sutherland, C. Sweeney, A. Poisson, N. Metzl, B. Tilbrook, N. Bates, R. Wanninkhof, R. A. Feely, C. Sabine, J. Olafsson, and Y. Nojiri (2002), Global sea–air CO_2 flux based on climatological surface ocean pCO_2 and seasonal biological and temperature effects. Deep-Sea Research 49:1601–1622.

Timmermans, M.-L., J. Toole, R. Krishfield, and P. Winsor (2008), Ice-Tethered Profiler observations of the double-diffusive staircase in the Canada Basin thermocline,J. Geophys. Res.,113, C00A02, doi:10.1029/2008JC004829.

Timmermans, M. L., R. Krishfield, S. Laney, and J. Toole (2010), Ice-Tethered Profiler measurements of dissolved oxygen under permanent ice cover in the AO. Journal of Atmospheric and Oceanic Technology, Vol. 27, 1936-1949. doi: 10.1175/ 2010JTECHO772.1.

Timmermans, M.-L., Sylvia Cole, and John Toole (2012), Horizontal Density Structure and Restratification of the Arctic Ocean Surface Layer. J. Phys. Oceanogr., 42, 659–668. doi: http://dx.doi.org/10.1175/JPO-D-11-0125.1

Toole, J. M., M.-L. Timmermans, D. K. Perovich, R. A. Krishfield, A. Proshutinsky, and J. A. Richter-Menge (2010), Influences of the ocean surface mixed layer and thermohaline

stratification on Arctic Sea ice in the central Canada Basin , J. Geophys. Res. , 115 , C10018, doi:10.1029/2009JC005660.

Toole, J.M., R.A. Krishfield, M.-L. Timmermans, and A. Proshutinsky (2011), The Ice-Tethered Profiler: Argo of the Arctic. Oceanography 24(3): 126–135, http://dx.doi.org/10.5670/oceanog.2011.64.

Top, Z., S. Martin, and P. Becker (1985), On the dissolved surface oxygen supersaturation in the Arctic, Geophys. Res. Lett., 12(12), 821–823.

Top, Z., S. Martin, and P. Becker (1988), A laboratory study of dissolved noble-gas anomaly due to ice formation, Geophys. Res. Lett., 15(8), 796–799.

Tremblay, J.-É., et al. (2011), Climate forcing multiplies biological productivity in the coastal Arctic Ocean, Geophys. Res. Lett., 38, L18604, doi:10.1029/2011GL0488 25.

Tremblay, J.-É., and J. Gagnon (2009), The effects of irradiance and nutrient supply on the productivity of Arctic waters: A perspective on climate change, in Influence of Climate Change on the Changing Arctic and Sub-Arctic Conditions, edited by J. J. Nihoul and A. Kostianoy, pp. 73–93, Springer, Netherlands.

Turk, D. Malacic, V. DeGrandpre, M.D. and W. R. McGillis. (2010), Carbon dioxide variability and air-sea fluxes in the northern Adriatic Sea, J. Ge-ophys. Res., 115, C10043, doi:10.1029/2009JC006.

Ulfsbo, A., N. Cassar, M. Korhonen, S. van Heuven, M. Hoppema, G. Kattner, and L. G. Anderson (2014), Late summer net community production in the central Arctic Ocean using multiple approaches. Global Biogeochemical Cycles, in press, doi:10.1002/2014GB004833.

Vancoppenolle, M., L. Bopp, G. Madec, J. Dunne, T. Ilyina, P. R. Halloran, and N. Steiner (2013), Future Arctic Ocean primary productivity from CMIP5 simulations: Uncertain outcome, but consistent mechanisms, Global Biogeochem. Cycles, 27, 605–619, doi:10.1002/gbc.20055.

van Heuven, S., D. Pierrot, J.W.B. Rae, E. Lewis, and D.W.R. Wallace (2011), MATLAB Program Developed for CO2 System Calculations. ORNL/CDIAC-105b. Carbon Dioxide Information Analysis Center, Oak Ridge National Laboratory, U.S. Department of Energy, Oak Ridge, Tennessee. doi: 10.3334/CDIAC/otg.CO2SYS_ MATLAB_v1.1

Walsh, J. J. (1991), Importance of continental margins in the marine bio- geochemical cycling of carbon and nitrogen, Nature, 350, 53–55.

Walsh, J. J., Premuzic, E. T., Gaffney, J. S., Rowe, G. T., Harbottle, G., Stoenner, R. W., Balsam, W. L., Betzer, P. R., and Macko, S. A (1985), Organic storage of CO_2 on the continental slope off the Mid-Atlantic bight, the southeastern Bering Sea, and the Peru coast, Deep-Sea Res., 32, 853–883.

Wanninkhof, R. (2014), Relationship between wind speed and gas exchange over the ocean revisited, Limnol. Oceanogr.: Methods Volume 12, Issue 6, pages 351–362, DOI: 10.4319/lom.2014.12.351.

Ward BB, Tuit CB, Jayakumar A, Rich JJ, Moffett J, (2008), Organic carbon, and not copper, controls denitrification in oxygen minimum zones of the ocean, Deep-Sea Res Part I 55: 1672–1683.

Wassmann, P., et al. (2006), Food webs and carbon flux in the Barents Sea, Prog. Oceanogr., 71(2–4), 232–287, doi:10.1016/j.pocean.2006.10.003.

Weiss, RF. (1974), Carbon dioxide in water and seawater: the solubility of a non-ideal gas. Marine Chemistry, 2:203-215.

Wheeler, P. A., Gosselin, M., Sherr, E., Thibault, D., Kirchman, D. L., Benner, R., Whitledge, T. E. (1996), Active cycling of organic carbon in the central Arctic Ocean. Nature, 380 (6576) (1996), pp. 697–699.

Winn, C. D., Mackenzie, F. T., Carillo, C. J., Sabine, C. L., and Karl, D. M (1994), Air-sea carbon dioxide exchange in the North Pacific Sub- tropical Gyre: Implications for the global carbon budget, Global Biogeochem. Cy., 8(2), 157–163.

Yamamoto-Kawai, M., M., F. A. McLaughlin, and E. C. Carmack (2011), Effects of ocean acidification, warming and melting of sea ice on aragonite saturation of the Canada Basin surface water, Geophys. Res. Lett., 38, L03601, doi:10.1029/2010GL045501.

Yamamoto-Kawai, M., McLaughlin, F. A., Carmack, E. C., Nishino, S., Shimada, K. and N. Kurita (2009a), Surface freshening of the Canada Basin, 2003–2007: River runoff versus sea ice meltwater, J. Geophys. Res., 114, C00A05, doi: 10.1029/ 2008JC005000.

Yamamoto-Kawai, M., F. A. McLaughlin, E. C. Carmack, S. Nishino, and K. Shimada (2009b), Aragonite Undersaturation in the Arctic Ocean: Effects of ocean acidification and sea ice melt, Science, 326,1098-1100, doi:10.1126/science. 1174190.

Yamamoto-Kawai, M., N. Tanaka, and S. Pivovarov (2005), Freshwater and brine behaviors in the Arctic Ocean deduced from historical data of $\delta^{18}O$ and alkalinity (1929-2002 A.D.), J. Geophys. Res., 110, C10003, doi:10.1029/2004JC 002793.

Zhang J., Lindsay R., Schweiger A., Steele M. (2013), The impact of an intense summer cyclone on 2012 Arctic sea-ice retreat. Geophys Res Lett. doi: 10.1002/grl.50190.

Zeebe, R. E. & Wolf-Gladrow, D. (2001), CO_2 in seawater: equilibrium, kinetics, isotopes. Oceanography series, vol. 65, pp. 1-346. Amsterdam, The Netherlands: Elsevier.